

1 **Insights into the diversity and function of DNA methyltransferases in**
2 **microeukaryotes using the model diatom *Phaeodactylum tricornutum***

3

4 Antoine Hoguin¹, Feng Yang², Agnès Groisillier², Chris Bowler¹, Auguste Genovesio¹,
5 Ouardia Ait-Mohamed^{1†*}, Fabio Rocha Jimenez Vieira^{1‡*} and Leila Tirichine^{2*}

6

7 ¹Institut de biologie de l'Ecole normale supérieure (IBENS), Ecole normale supérieure,
8 CNRS, INSERM, PSL Université Paris 75005 Paris, France

9 ² Nantes Université, CNRS, US2B, UMR 6286, F-44000 Nantes, France

10

11 [†]Current affiliation: Immunity and Cancer Department, Institut Curie, PSL Research
12 University, INSERM U932, 75005 Paris, France

13 [‡]Current affiliation: Laboratory of Computational and Quantitative Biology - LCQB -
14 UMR 7238 CNRS - Sorbonne Université. Institut de Biologie Paris Seine. 75005 Paris

15

16

17

18 * Authors for correspondence: tirichine-l@univ-nantes.fr,
19 fabio.rocha_jimenez_vieira@sorbonne-universite.fr, ouardia.ait-mohamed@curie.fr

20

21

22

23

24

25

26

27

28

29

30

31

32

33

34

35

36 **Abstract**

37 Cytosine methylation is an important epigenetic mark involved in the transcriptional
38 control of transposable elements in mammals, plants and fungi. The Stramenopiles-
39 Alveolate-Rhizaria lineages are a major group of ecologically important marine
40 microeukaryotes that include the main phytoplankton groups diatoms and
41 dinoflagellates. However, little is known about their DNA methyltransferase diversity.
42 Here, we performed an *in-silico* analysis of DNA methyltransferases found in marine
43 microeukaryotes and showed that they encode divergent DNMT3, DNMT4, DNMT5
44 and DNMT6 enzymes. Furthermore, we revealed three novel classes of enzymes
45 within the DNMT5 family. Using a CRISPR/Cas9 strategy we demonstrated that the
46 loss of the DNMT5a gene correlates with a global depletion of DNA methylation and
47 overexpression of young transposable elements in the model diatom *Phaeodactylum*
48 *tricornutum*. The study provides a pioneering view of the structure and function of a
49 DNMT family in the SAR supergroup using an attractive model species.

50

51 **Introduction**

52 In eukaryotes the methylation of the fifth carbon of cytosine (5mC) is a well-known
53 epigenetic mark associated with transcriptional repression. It has been implicated in a
54 wide range of cellular processes including the stability of repeat rich centromeric and
55 telomeric regions as well as in repression of transposable element (TEs) expression^{1–}
56 ⁴. 5mC is deposited by DNA methyltransferases (DNMTs) capable of *de novo*
57 methylation and is propagated through subsequent cell division by maintenance DNMT
58 enzymes. Eukaryotes have acquired a diverse set of DNMTs by horizontal gene
59 transfer of bacterial DNA cytosine methyltransferase (DCM) involved in the restriction-
60 methylation system ⁵. All DNMTs contain a catalytic protein domain composed of ten
61 conserved motifs (annotated I to X) that provide binding affinity to the DNA substrate
62 and the methyl donor cofactor S-Adenosyl methionine (SAM) to process the transfer
63 of a methyl group to unmethylated cytosines ^{6,7}. DNMTs have further diversified over
64 evolutionary time scales in eukaryote lineages and acquired chromatin associated
65 recognition and binding domains giving rise to a wide diversity of DNA methylation
66 patterns ^{8,9}.

67 The loss and gain of DNMTs have been associated with profound divergence in
68 cell biology and control of gene expression. To date, six main eukaryotic DNMT
69 families have been described and named DNMT1, DNMT2, DNMT3, DNMT4, DNMT5
70 and DNMT6 ^{10,11}. In Metazoans, the combined activity of the DNMT3 family and
71 DNMT1 enzymes allow the deposition and the maintenance of DNA methylation
72 patterns during the successive developmental waves of DNA demethylation and
73 remethylation¹². Zebrafish possess six “dnmt3 family” *de novo* methyltransferase
74 genes, *dnmt3–dnmt8*. This group includes both orthologs of mammalian *dnmt3a* and
75 *dnmt3b* as well as fish-specific genes with no mammalian orthologs¹³. In fungi, the DNA
76 methylation machinery consists in a maintenance activity by DNMT1/DIM2, as in
77 *Neurospora crassa*¹⁴, or by the activity of ATPase-DNMT5 enzymes as reported in
78 *Cryptococcus neoformans* ^{11,15}. The DNMT5 enzyme also correlates with a heavy
79 histone linker DNA methylation landscape in *Micromonas pusilla*, the pelagophyte
80 *Aureococcus annophagefferens* and the haptophyte *Emiliania huxleyi*¹¹. Fungal
81 DNMT4 relatives are involved in the DNA methylation related process known as
82 Repeat-Induced Point Mutation (RIP) and Methylation Induced Premeiotically (MIP)
83 that leads to TE extinction and/or stage specific repression as observed in *Aspergillus*
84 and *Neurospora* species ^{16–19}.

85 Losses and lineage specific duplication of DNMT1 and DNMT3 have occurred
86 during insect evolution, such as in Diptera lineages²⁰, leading to secondary loss of
87 global 5mC methylation. In plants, the acquisition of novel DNMT1 proteins named
88 Chromomethylases (CMTs) and the divergence of the DNMT3 family led to the
89 spreading of the asymmetrical non-CG patterns of DNA methylation that is extensively
90 found in angiosperms²¹⁻²³. DNMT2 is known to methylate tRNAs to yield ribo-5-
91 methylcytidine (rm5C) in a range of eukaryotic organisms, including humans, mice,
92 *Arabidopsis thaliana*, and *Drosophila melanogaster*²⁴. It is characterized by its
93 cytoplasmic localization that contrasts with the exclusively nuclear localization of
94 Dnmt1 and Dnmt3²⁵. Lastly, DNMT6 has been found in *Chlorophyta*, *Haptophyta*,
95 *Ochrophyta*, diatoms and dinoflagellates (e.g., *Symbiodinium kawagutii* and
96 *Symbiodinium minutum*)^{10,11,26,27} but its function remains elusive. Importantly, 5mC is
97 increasingly reported in eukaryotes of the Stramenopiles-Alveolate-Rhizaria (SAR)
98 lineages as in dinoflagellates²⁶, diatoms²⁷ and kelps²⁸. However, because of the severe
99 underrepresentation of marine unicellular eukaryotes in modern sequencing
100 databases, our understanding of the DNA methylation machinery in these organisms
101 remains scarce.

102 Diatoms are a dominant, abundant, and highly diverse group of unicellular brown
103 microalgae (from 2 to 200 μ m) of the stramenopile lineage. It is estimated that diatoms
104 are responsible for nearly 20% of primary production on earth^{29,30}. They are known to
105 dominate marine polar areas and are major contributors of phytoplankton oceanic
106 blooms. To date, 5mC has been reported in four diatoms, namely the centrics
107 *Thalassiosira pseudonana*¹¹ and *Cyclotella cryptica*³¹, as well as in *Fragilariaopsis*
108 *cylindrus*¹¹ and *Phaeodactylum tricornutum*^{11,27}. Diatom methylation patterns strongly
109 contrasts with the patterns observed in animals but also dinoflagellates and plants³².
110 Firstly, in *P. tricornutum*, *T. pseudonana* and *F. cylindrus*, total levels of DNA
111 methylation range from 8% to as low as 1% of cytosines in the CG context¹¹ over
112 repeats and TEs usually (but not exclusively) concentrated in telomeric regions^{11,27}.
113 Non-CG methylation is also detected but is scarce. Diatom genomes are therefore
114 predominantly composed of isolated highly CG methylated TE islands in an otherwise
115 unmethylated genome and to that regard are remarkably like fungal methylation
116 profiles. In all diatoms examined so far, methylated TEs often have low expression
117 ^{11,27,31}. This is remarkably consistent with the repressive role of DNA methylation in
118 other eukaryotes and further traces back 5mC-mediated control of TE expression to

119 the last eukaryotic common ancestor. Nonetheless, direct evidence of the repressive
120 role of 5mC on TEs in diatoms is lacking. Diatom genomes contain predicted proteins
121 similar to members of the DNMT2, DNMT3, DNMT4, DNMT5 and DNMT6 family^{11,33}.
122 The conservation of their domain composition across eukaryotic groups as in the yeast
123 *Cryptococcus neoformans* suggests that diatom DNMT5-like C5-MTases play a
124 conserved and specific role in DNA methylation^{11,15}. However, the functions of the
125 DNMTs reported in diatoms have not been characterized *in vivo*.

126

127 Recent advances in high throughput RNA sequencing technologies led to the
128 development of the Microbial Eukaryote Transcriptome Sequencing Project
129 (MMETSP)³⁴. The MMETSP concatenates more than 650 transcriptomes from diverse
130 microeukaryote lineages such as diatoms and dinoflagellates, making it the biggest
131 sequence database for transcriptomes from individual marine microeukaryote. Here,
132 utilizing the newly defined enhanced Domain Architecture Framework (eDAF)
133 methodology³⁵, we first explored the structural and phylogenetic diversity of DNMT
134 sequences in marine microeukaryotes from the publicly available MMETSP
135 sequencing databases. Using an integrative approach with available genomes and
136 phylogenetic studies, we provide a DNMT phylogeny focused on the structural and
137 domain diversity found in microeukaryote enzymes and discuss their evolutionary
138 origins. We define, in the DNMT5 family, the sub-families DNMT5a, b and c enzymes,
139 based on structure and phylogenetic assessment. The presence of the predicted
140 DNMT5 family diversity remarkably contrasts with the apparent lack of DNMT1 in most
141 of the MMETSP and microeukaryote databases. Using CRISPR/Cas9 genome editing,
142 we present the functional characterization of the DNMT5a sub-family in the model
143 diatom *P. tricornutum* demonstrating, to our knowledge for the first time in any SAR,
144 the role of this family in the repression of TEs in an early diverging eukaryote lineage.

145

146 **Results**

147 **Diversity of DNMT5 methyltransferases in microeukaryotes**

148 To capture the diversity of 5-cytosine DNA methyltransferases encoded in
149 microalgae, we applied a relaxed HMMER search (e-value=1 as the cut-off threshold)
150 for the PFAM DNMT (PF00145) domain on transcriptomes from the MMETSP
151 database. This approach successfully detects more than 99% of true positives³⁶. In
152 this study we focused on the DNMT1, DNMT3, DNMT4, DNMT5 and DNMT6 gene

153 families that are known or represent putative DNA modifying enzymes. We retained
154 sequences showing conserved DNMT domains and depicted their domain structures
155 by eDAF curation³⁵. We built a representative phylogeny of DNA methyltransferases
156 based on the alignment of conserved DNMT motifs (Fig. 1a, Additional File 1: Fig. S1,
157 Additional File 2: Table S1). Since DNMT2 is an aspartic acid transfer RNA
158 methyltransferase²⁵, published microalgal DNMT2 sequences were used as additional
159 sequences for phylogenetic analysis. The tree construction exploited the stability of
160 Bayesian approaches to deal with the fast evolution rates observed in our DNMT
161 sequences. Methods based on posterior probabilities present more stable support
162 values than random sampling algorithms when facing high mutation rates³⁷⁻³⁹.
163 We found three gene families related to the DNMT5 clade of enzymes that we named
164 DNMT5a, DNMT5b and DNMT5c (Fig. 1a). The sequence alignments show high
165 homology in the functional DNMT motifs (I-IV, VII and X) that contain the SAM binding
166 and catalytic domains within DNMT5s (Additional File 1: Fig. S2). We noticed that the
167 DNMT5 SAM-binding phenylalanine found in the catalytic motif IV of other DNMTs is
168 replaced by a serine. The three DNMT5 families form a supported group of enzymes
169 (posterior probabilities 0.94). The DNMT5a and DNMT5b clades are well supported
170 (posterior probabilities of 0.98 and 0.97, respectively). The DNMT5c family is however
171 less supported (posterior probability of 0.88). The relationships between the
172 DNMT5a,b,c sequences are however unresolved as the DNMT5a,b branch is poorly
173 supported (posterior probability of 0.51). Of note, DNMT5a is found in distantly related
174 eukaryote lineages. We found 76 species with at least one DNMT5 orthologue. We
175 found a DNMT5a in the green alga *Tetraselmis astigmata* but also in haptophytes and
176 the marine photosynthetic excavate euglenozoa *Eutreptiella gymnastica*. The
177 DNMT5a family is also found in strameopiles, including diatoms, bolidomonas,
178 pelagophytes and dictiochophytes, as well as in fungi (former *Cryptococcus* DNMT5-
179 related enzymes) (Fig. 1a, Additional File 2: Table S2). This might suggest that
180 DNMT5a is the ancestral DNMT5 in eukaryotes. The DNMT5b enzyme is found in
181 diatoms, *Bolidomonas pacifica* and haptophytes. *Emiliania huxleyi* DNMT5 enzymes
182 are not found in other haptophytes in the MMETSP database. In addition, the nodal
183 supports and topologies of *E. huxleyi* DNMT5a and DNMT5b enzymes are not very
184 convincing considering their branching pattern with the other DNMT5a and b families
185 (Additional File 1: Fig. S1). Within diatoms, genomes from both *F. cylindrus* and
186 *Synedra* contain DNMT5a and a DNMT5b gene copies (Additional File 2: Table S3)

187 but lineage specific loss of DNMT5a is also observed in some centric species. This
188 suggests that stramenopiles show an ancestral duplication of DNMT5s, which are
189 differentially retained as DNMT5b or DNMT5a in diatoms and *B. pacifica*. Haptophyte
190 DNMT5s could be of lateral gene transfer origin, as in other microalgae. DNMT5c
191 enzymes are specific to dinoflagellates that are known to have very fast evolutionary
192 rates and likely divergent base/amino acid compositions. Dinoflagellate DNMT5c
193 sequences may thus represent a highly divergent DNMT5a subgroup that our
194 phylogeny failed to associate with other DNMT5s.

195 We found that the DNMT5a and b families share a C-terminal SNF2-type
196 DEXDc/HELICc helicase domain composed of two helicases complemented or not by
197 a RING finger domain (Fig. 1b, Additional File 2: Table S4). We found that DNMT5b
198 enzymes display unique features. First, among them, 14 contain an N-terminal laminin
199 B receptor domain as in *T. pseudonana* (Fig. 1b, Additional File 2: Table S4). Also,
200 other DNMT5b enzymes contain N-terminal CpG methyl binding domains, as well as
201 HAND structure domains and methyl-lysine and methyl-arginine TUDOR binding
202 domains (Additional File 2: Table S4). Finally, their DNMT domain is longer compared
203 to the DNMT5a,c due to the presence of spacer sequences between motifs. These
204 differences in structure may highlight functional diversity between the DNMT5
205 subfamilies and is consistent with the duplication followed by divergence hypothesis
206 described above. Accordingly, the DNMT5c family also diverged compared to the
207 DNMT5a and b enzymes at the protein domain composition. It is indeed characterized
208 by a long (~1000 amino-acids) N-terminal sequence with no annotated functional
209 domains (Fig. 1b, Additional File 2: Table S4).

210

211 **The DNMT4 family: a DNMT1 divergent paraphyletic gene family**

212 In our phylogeny analysis, the DNMT4 and DNMT1 clades form a poorly
213 supported gene family, as previously described^{11,40} (Fig. 1a, Additional File 1: Fig. S1).
214 DNMT1s are maintenance enzymes in eukaryotes that often associate a DNMT
215 catalytic domain with chromatin binding domains such as Bromo-Adjacent Homology
216 (BAH) domains, Plant HomeoDomains (PHDs), chromodomains and domains required
217 for interaction with accessory proteins. DNMT4 enzymes are related to DIM2 enzymes
218 in fungi⁴⁰ and are involved in the MIP and RIP processes. Interestingly, two DNMT4
219 enzymes were also described in the pennate diatom *F. cylindrus* and the centric diatom
220 *T. pseudonana* based on a previous phylogenetic analysis of DNMT enzymes in

221 microalgae ¹⁰. We first confirmed that orthologues of *T. pseudonana* DNMT4 enzymes
222 are widespread in diatom transcriptomes and genomes. A total of 31 diatoms out of
223 60, pennate and centric species express or encode at least one DNMT4 related
224 transcript (Additional File 2: Table S3). This finding suggests that the family is ancestral
225 in diatoms. In our analysis, no DNMT4 enzymes were found in other species. *T.*
226 *pseudonana* DNMT4 and RID can be mutually found by reciprocal BLAST best hit
227 analysis (data not shown). Phylogenetic analysis indicates that RID and diatom
228 DNMT4s may form a moderately supported monophyletic family of enzymes (Fig. 1a).
229 At the structural level, both RID and diatom DNMT4 enzymes diverged compared to
230 DNMT1 enzymes, and also between each other. Most diatom DNMT4 enzymes are
231 composed of a single DNMT domain as in *T. pseudonana*, which also contrasts with
232 fungal enzymes (Fig. 1b, Additional File 2: Table S4). Nonetheless, nine diatom
233 DNMT4 proteins possess an additional N-terminal chromodomain as observed in
234 *Thalassiosira miniscula* (Fig. 1b, Additional File 2: Table S3 and S4). We also found
235 two putative DNMT1-like enzymes in the transcriptomic database of two
236 *Raphidophyceae* brown microalgae: *Heterosigma akashiwo* and *Chatonella subsala*.
237 They are composed of a conserved DNMT domain and a plant homeodomain (PHD)
238 (Fig. 1b, Additional File 1: Fig. S1, Additional File 2: Table S4) but poorly define a
239 monophyletic gene family with either DNMT1s or DNMT4s. Together, these data rather
240 suggest that diatoms, fungi and raphidophyceae enzymes are paraphyletic DNMT1-
241 divergent gene families.

242 Interestingly, we found a DNMT1-related enzyme in three haptophyte species out
243 of four (*Gephyrocapsa oceanica*, *Isochrysis*.sp-CCMP1324 and *Coccolithus*
244 *pelagicus*) from the MMETSP database that cluster with annotated CMTs found in the
245 coccolithophore *E. huxleyi* (Fig. 1a, Additional File 1: Fig. S1). We found that the
246 enzymes of *Gephyrocapsa oceanica* (CAMPEP_0188208858), *Isochrysis*-CCMP1324
247 (CAMPEP_0188844028) and *Emiliania huxleyi* (jgi_215571) have DNMT1-like
248 structures with a Replication Foci Domain (RFD) followed by a BAH (in *Emiliania*
249 *huxleyi* only) and a conserved DNMT domain (Fig. 1b, Additional File 2: Table S4).
250 Haptophyte enzymes seem to distantly relate to the conserved green algal CMT
251 (hCMT2) enzymes (Fig. 1a, Additional File 1: Fig. S1).

252 We detected DNMT1/MET1 transcripts encoding proteins similar to the plant
253 MET1 enzyme in seven green algae species from MMETSP, such as in some
254 *Chlamydomonas* species (Fig. 1b, Additional File 1: Fig. S1, Additional File 2: Table

255 S2), suggesting that the DNMT1 family is ancestral in plant evolution and could have
256 been lost in other green algal lineages.

257

258 **The DNMT3 and DNMT6 methyltransferases are abundant in diatoms and lack 259 chromatin associated domains**

260 Our data indicate that the DNMT3 family is not particularly frequent in
261 microalgae (Fig. 2, Additional File 2: Table S2). DNMT3 is absent in most
262 stramenopiles except in diatoms; for which genomic and transcriptomic data strongly
263 support its presence (Additional File 2: Table S3). DNMT3 seems absent in the studied
264 haptophytes (Fig. 2, Additional File 2: Table S2). Only one transcript from the
265 cryptomonad *Goniomonas pacifica* could be annotated as DNMT3. In addition, we
266 could not identify DNMT3 enzymes in any green algae in MMETSP, although it is
267 present in red algae as it is found in the genomes of *Cyanidioschyzon merolae* and
268 *Galdieria sulphuraria* (Fig. 2, Additional File 2: Table S2). We also report several
269 additional DNMT3 transcripts in dinoflagellates, as previously described²⁶ (Fig. 2,
270 Additional File 2: Table S2). Upon alignment, dinoflagellate DNMT3 enzymes
271 (including former annotated enzymes²⁶) and *Goniomonas pacifica* DNMT3s are closely
272 related to those from red algae but diverge from other DNMT3s, while diatoms display
273 their own DNMT3 family (Additional File 1: Fig. S1). This suggests that the DNMT3
274 family was iteratively lost and acquired several times during microalgal evolution. As
275 observed in *P. tricornutum*, DNMT3 enzymes found in microalgae, all lack chromatin
276 associated domains (Fig. 1b, Additional File 2: Table S4). This contrasts with
277 mammalian DNMT3s⁴¹ that interact with histone post-translational modifications.

278 DNMT6 enzymes were found among the most widespread DNMTs in
279 microeukaryotes. We found a DNMT6 transcript in the MMETSP transcriptomes of
280 three *Tetraselmis* green algae and seven dinoflagellates (Fig. 2, Additional File 2:
281 Table S2). In addition, DNMT6 is distributed extensively in stramenopiles, including
282 *Dictyochophyceae*, *Crysophyceae* and *Pelagophyceae* (Fig. 2, Additional File 2: Table
283 S2). In diatoms, DNMT6 is very abundant (Additional File 2: Table S3). DNMT6 is also
284 present in the non-photosynthetic labyrinthulomycetes *Aplanochytrium stocchinoi* and
285 probably in *Aplanochytrium keurgelense* (Fig. 2, Additional File 2: Table S2). In
286 addition, our data strongly support the presence of DNMT6 orthologues in the major
287 *Chromalveolata* lineage of *Rhizaria* (Fig. 2, Additional File 2: Table S2), as suggested
288 in previous reports²⁶. DNMT6 enzymes are mostly homogeneous and do not contain

289 chromatin associated signatures, as in *P. tricornutum* DNMT6 and DNMT3 (Fig. 1b,
290 Additional File 2: Table S4). Finally, monophyletic relationships within the DNMT6
291 family and between microeukaryotes could not be solved (Additional File 1: Fig. S1).

292

293 **Single base resolution of DNA methylation in *P. tricornutum* DNMT5:KO lines**

294 The pennate diatom *P. tricornutum* is the model diatom species that we and
295 others use to study the epigenomic landscape in diatoms, shedding light into the
296 conservation and divergence of DNA methylation patterns in early diverging
297 eukaryotes^{27,42}. The *P. tricornutum* genome encodes DNMT3 (Phatr3_J47136),
298 DNMT6 (Phatr3_J47357) and DNMT5a (Phatr3_EG02369) orthologues in single
299 copies but lacks the DNMT4 and DNMT5b orthologues found in other diatoms
300 (Additional File 2: Table S3). We asked whether any of these DNMTs have DNA
301 methylation function(s) *in vivo*. Using a CRISPR/Cas9-mediated knockout approach,
302 we screened *P. tricornutum* for DNMT loss of function mutants (see material and
303 methods). In this work, we report five independent mutants with homozygous out of
304 frame deletions generating premature STOP codons in the coding sequence of
305 DNMT5a named 'M23', 'M25', '7C6', '7C7' and 'M26' DNMT5:KOs. In this study, the
306 mutants M23 and M25 were further exploited (Additional File 1: Fig. S3a). No DNMT3
307 or DNMT6 mutations could be generated using the CRISPR/Cas9 editing strategy.

308 Using sets of primer pairs targeting the DNMT domain as well as the DEADX
309 helicase-SNF2 like domain of DNMT5 transcripts, we detected by RT-qPCR a 4- to 5-
310 fold loss in mRNA levels in both M23 and M25 cell lines (Additional File 1: Fig. S3b,
311 Additional File 2: Table S5). 5mC dot blot screening revealed that all DNMT5:KOs had
312 a 4-5 fold loss of DNA methylation compared to the Pt18.6 reference ('wild-type')
313 (Additional File 1: Fig. S3c,d), consistent with the putative role of DNMT5 in maintaining
314 DNA methylation patterns in diatoms.

315 To generate a quantitative single base resolution of DNA methylation loss in
316 DNMT5:KOs, we performed whole genome bisulfite sequencing in M23, M25
317 (considered as two biological replicates) and the reference, Pt18.6 line. We filtered
318 cytosines by coverage depth considering a 5X coverage in all cell lines as a threshold
319 and computed CG methylation levels in TEs and genes. We found that CG methylation
320 is severely impaired in M23 and M25 compared to Pt18.6 cell lines (Fig. 3a,b,
321 Additional File 2: Table S6). This is particularly observed within TEs that are the targets
322 of DNA methylation in *P. tricornutum* (Fig. 3a, b). Non-CG (CHH, CHG) methylation is

323 low in all cell lines confirming the dominance of CG methylation in *P. tricornutum* (data
324 not shown). To get a quantitative view of the loss of DNA methylation in DNMT5:KOs,
325 we defined differentially methylated regions (DMRs). We computed DMRs between
326 DNMT5:KOs and WT lines using the bins built-in DMRcaller⁴³ tools considering 100
327 bp bins with a minimal difference of +/- 20% DNA methylation at CGs (5X coverage) in
328 mutants compared to the Pt18.6 line. Those thresholds were used based on the
329 minimum coverage per cytosine and the methylation characteristics in our sequencing
330 data (Additional file 1: Fig. S4a,b). We identified 1715 and 1720 CG DMRs in M23 and
331 M25, respectively (Additional File 2: Table S7 and S8), of which 96% are shared
332 between both mutants and show a consistent loss of DNA methylation upon knockout
333 of DNMT5a (Fig. 3c), referred in this study as common hypoDMRs. We did not find
334 non-CG DMRs in line with the absence of a clear global pattern in any of the cell lines
335 (data not shown). CG common hypoDMRs cover ~0.8% of the *P. tricornutum* genome.
336 According to the distribution of DNA methylation in the reference strain, we found that
337 14.90% (n=454) of annotated TEs are found within common hypoDMRs (Fig. 3d,
338 Additional File 2: Table S9). In order to take into account the possible methylation loss
339 occurring in regulatory regions, gene and TE coordinates were extended by 500 bp
340 and 1 kb, respectively, upstream and downstream of their start and end sites,
341 considering that intergenic length in *P. tricornutum* varies between 1 kb and 1.5 kb²⁷.
342 As a result, respectively 7.76% and 12.23% of TEs are found within 500 bp and 1 kb
343 of common hypoDMR coordinates (Fig. 3d, Additional File 2: Table S9). Consistent
344 with their low level of CG DNA methylation observed in both cell lines, we found a
345 comparatively low overlap of common hypoDMRs with genes or their regulatory
346 regions (Fig. 3d, Additional File 2: Table S9). We then asked whether these common
347 hypoDMRs associate with known regions marked by histone post-translational
348 modifications. Genomic coordinates of common hypoDMRs overlapped with
349 previously mapped histone post-translational modification peaks⁴². The number of
350 common hypoDMRs overlapping with each combination of histone marks is shown in
351 Fig. 3e. Interestingly, we found that between 80 and 90% of these common hypoDMRs
352 (set size >1500, Fig. 3e) overlap with known regions marked by H3K27me3, H3K9me3
353 or H3K9me2 defined in the reference Pt18.6 line⁴². In addition, 963 (53%) of the
354 common hypoDMRs are found within regions co-marked by all three repressive histone
355 marks (Fig. 3e). This is consistent with the observation that highly methylated regions
356 described by restriction methylation-sensitive sequencing (Mcrbc-Chip) also associate

357 with such histone marks²⁷. Our data are consistent with a global loss of DNA
358 methylation in DNMT5:KO at TE-rich DNA methylated-H3K27me3, H3K9me2 and
359 H3K9me3 marked regions in the *P. tricornutum* genome.

360 **Gene and TE expression in the absence of DNMT5a in *P. tricornutum***

361 The control of TEs by the DNA methyltransferase family is a key unifying feature
362 within eukaryotes². We hence monitored the transcriptional effect of the loss of
363 DNMT5a on genes in M23 and M25 backgrounds by whole RNA high throughput
364 sequencing (Material and Methods). Given the high level of DNA methylation observed
365 at TEs compared to genes, we asked whether our RNAseq data captured any TE
366 overexpression that could be linked to hypoDMRs. We thus analyzed TE-gene
367 transcripts that correspond to the expression of TE open reading frames (i.e., encoding
368 reverse transcriptase and integrases) but also genes with TE insertions (Fig. 4a),
369 domesticated TEs and mis-annotated TE loci^{27,44}. To identify the most significant
370 changes in mRNA levels, we focused our analysis on genes and TE-genes showing a
371 significant 2-fold induction or reduction of expression in mutants compared to the
372 reference line ($|LFC| > 1$ and an FDR < 0.01 , Additional File 2: Table S10). In M23 and
373 M25, respectively, a total of 1732 and 806 genes and TE-genes are overexpressed
374 while downregulation was observed for 1152 and 248 genes and TE-genes (Fig. 4b).
375 Stable expression ($-1 < LFC < 1$ and FDR < 0.01) is observed for 943 genes and TE-
376 genes in M23 and 216 genes and TE-genes in M25. We found that 557 genes are
377 overexpressed in both cell lines ($M23 \cap M25$). A total of 225 genes are overexpressed
378 in M25 only (M25-spe) and 1126 are overexpressed in M23 only (M23-spe).
379 Significantly upregulated genes in both mutants show consistent overexpression levels
380 (Fig. 4c).

381 We found that 338 TE-genes are upregulated in both mutants (Fig. 4d) which
382 correspond to 56% of overexpressed TE-genes. Gene ontology (GO) analysis showed
383 that the upregulated TE-genes are enriched in DNA integration biological function
384 indicating that they mainly correspond to *bona fide* TE annotations (Fig. 4d). While only
385 219 (16%) of protein coding genes are overexpressed in both mutants and show clear
386 enrichment for GOs associated with protein folding as well as nucleotide phosphate
387 metabolism and nucleotide binding activity (Fig. 4e, Additional File 2: Table S11). This
388 is typified by the overexpression of chaperone DnaJ domain-containing proteins and
389 Hsp90-like proteins (Additional File 2: Table S12). The downregulation of genes was

390 not consistent between M23 and M25 as only 35 genes and 16 TE-genes are
391 downregulated in both cell lines (Fig. 4f,g, Additional File 2: Table S13). Expression
392 levels of 12 genes was confirmed by qPCR in the M23 cell line, including DnaJ and
393 HSP90-like protein coding genes mentioned previously (Additional File 1: Fig. S5a,b,
394 Additional File 2: Table S15). Only two genes showed similar expression in M25 (data
395 not shown).

396 DNMT5a is among the downregulated genes in both mutants (Additional File 2:
397 Table S13), consistent with qCPR results. GO annotations of upregulated genes in
398 M23 only (M23-spe genes) are enriched for protein catabolic processes while M25-spe
399 genes are involved in protein synthesis processes (data not shown). GOs of genes
400 downregulated in M23 only (M23-spe) showed enrichment for ion-transport related
401 functions and the M25-spe showed enrichment for RNA processing and protein
402 transport (data not shown). This indicates that DNMT5:KO are transcriptionally
403 distinct but TE-gene regulation showed more consistent overexpression. Of note, this
404 is in line with the hypothesis that TEs and not genes are directly regulated by DNA
405 methylation in *P. tricornutum*.

406

407 **Relationship between CG methylation and expression of TE-genes in *P.*
408 *tricornutum***

409 The observed overexpression of TEs in DNMT5:KO could be directly due to the
410 loss of DNA methylation. To test this, we first determined DNA methylation levels in
411 the 600 upregulated TE-genes in the DNMT5:KO lines (Fig. 5a). For each TE, we also
412 computed the mean-centered normalized LFC (z-score) for each of the M23 and M25
413 lines (Fig. 5a). We found that the TE-genes with the highest LFC (z-score >2) in the
414 mutants are associated with higher DNA methylation levels in the reference strain. This
415 is the case for each mutant independently, indicating that TEs with the highest
416 upregulation in the DNMT5:KO lines are direct targets of DNA methylation in the
417 reference strain.

418 We then assessed the relationship between upregulated TE-genes and the common
419 hypoDMRs, and found that 62% of upregulated TE-genes are found within these DMRs
420 (Fig. 5b). Importantly, this was the case only for TE-genes with overexpression in both
421 cell lines (M23 ∩ M25) and not for M23-spe and M25-spe upregulated TE-genes (Fig.

422 5b). This also means that 40% of upregulated TE-genes cannot be explained by the
423 loss of DNA methylation alone. Similarly, downregulation and stable expression is not
424 associated with common hypoDMRs (Fig. 5b). This shows that TE-genes with
425 consistent upregulation are specifically due to the loss of DNA methylation while other
426 TE-gene misregulation is due to cell line specific DNA methylation-independent
427 regulation. Among the 128 upregulated TE-genes in both mutants that are not direct
428 targets of DNA methylation, we found a common hypoDMR in the regulatory region of
429 42 (in M23) and 15 TE-genes (in M25), respectively, indicating that DNA methylation
430 loss at these regions was also responsible for their upregulation (Fig. 5c).

431 Next, we assessed TE families as annotated previously⁴⁴ (Fig. 5d). We find that
432 overexpressed TE-genes are mostly represented by “Copia-like in diatoms” (CoDi)
433 retrotransposons of the CoDi1, CoDi2, CoDi4 and CoDi5 families with a minority of
434 DNA transposons as the PiggyBack family (Fig. 5d). We notice that the TE families
435 are found in similar proportions among TEs that overlap the common hypoDMRs and
436 those that do not. However, when we compared TE lengths, TEs that are upregulated
437 and overlap with common hypoDMRs are longer than upregulated TEs that are not
438 overlapping with hypoDMRs (Fig. 5e). This suggests that younger TEs tend to be direct
439 targets of DNA methylation compared to evolutionary older TEs family members.
440 Subsequently, loss of DNA methylation causes upregulation of mainly younger TEs.
441 Filloromo et al.⁴⁵ recently described 85 long-LTR-copia-like (LTR-copia) TEs based on
442 reannotation of the *P. tricornutum* genome by Oxford Nanopore Technologies long-
443 read sequencing. Such TEs are considered as potentially still active⁴⁵. They are
444 represented by “Copia-like in diatoms” (CoDi) of the CoDi5, CoDi4 and CoDi2
445 families⁴⁵ that corresponds to the TE families found overexpressed in our datasets (Fig.
446 5d). Accordingly, we found that 75/85 of LTR-copia are targets of DNA methylation and
447 are associated with common hypoDMRs (Additional File 2: Table S14). In addition, by
448 overlapping TE-genes and genomic locations of LTR-copia, we found that 61/75 of
449 LTR-copia are overexpressed in both mutants (Additional File 2: Table S14). Of note,
450 our RNAseq data thus also support the presence of these new TEs in the reference
451 Pt1.86 cell line as potentially still active elements. An example of upregulation at LTR-
452 copia is shown in Fig. 5f. Additional shorter TEs with overexpression also belong to
453 CoDi5, CoDi4 and CoDi2 TE categories suggesting that an active expression might

454 still remain. Altogether, this strongly suggests that DNA methylation is involved in the
455 repression of young TEs in the *P. tricornutum* genome.

456

457 **Discussion**

458 Studies on the evolutionary history of DNMTs have established that the DNA
459 methylation machinery diverged among eukaryotes along with their respective DNA
460 methylation patterns^{2,11}. However, the diversity of DNMTs found in SAR lineages is
461 underexplored due to the lack of representative sequences. Based on MMETSP
462 transcriptomes, we set out to explore the diversity and phylogeny of DNMTs in early
463 diverging eukaryotes. Besides the absence of genomic sequences, the MMETSP
464 database only encompasses expressed transcripts from cultured organisms and is
465 thus deprived of lowly expressed genes and condition-specific expressed genes.
466 Absence of a given gene family within a species should therefore be interpreted
467 accordingly. When our analysis found multiple distinct transcripts sharing the same
468 DNMT subfamily, as in diatoms, we used the most probable open reading frame
469 translation of the transcripts using eDAF curation to produce our phylogenetic tree.
470 However, without genomic annotations we cannot rule out that such transcripts result
471 from alternative transcription originating from a single gene or multi-copy gene families.
472 Our data are best interpreted at the lineage level when multiple transcripts and
473 annotated genes, whenever possible, are available, rather than at the species-specific
474 level.

475 We nonetheless confirm that stramenopiles and dinoflagellates encode a
476 divergent set of DNMT proteins including DNMT3 and DNMT6 which have no
477 chromatin associated domains. In addition, our study independently reports the same
478 DNMT6 enzymes found in the raphidophyceae, *Bigelowella natans* and
479 *Aplanochytrium stochhinoi* by earlier work although not specified by the authors²⁶. As
480 reported in trypanosomes¹⁰, we suggest that DNMT6 likely emerged prior to the
481 *Chromalveolata* radiation. In trypanosomes, its presence in several lineages does not
482 predict DNA methylation *per se* and must be further investigated⁴⁶.

483 The DNMT5 enzymes are also very well represented both at the genomic and
484 transcriptomic levels, even outside the SARs, and are thus likely ancestral to
485 eukaryotes. We show here that the DNMT domains among the different DNMT5s are
486 conserved but show a divergence compared to other DNMTs, thus supporting a

487 common evolutionary origin for all DNMT5 enzymes. The DNMT5b subfamily likely
488 emerged by gene duplication followed by divergence, as observed in diatoms. This
489 scenario is supported by the presence of both DNMT5a and b orthologues in the
490 genome of *F. cylindrus* and *Synedra* species. DNMT5b enzymes could be
491 multifunctional enzymes as suggested by the presence of N-terminal HAND domains
492 found in chromatin remodelers⁴⁷, TUDOR domains found in histone modifying
493 enzymes, histone post-translational modification readers⁴⁸ as well as small RNA
494 interacting proteins^{49,50} and an SNF2 ATPase domain¹¹ which plays a chaperone-like
495 enzyme-remodeling role important for DNA methylation and its targeting to specific
496 sites^{15,51}. DNMT5c enzymes are likely very divergent DNMT5a enzymes that lack ATP-
497 ase SNF domains. The diversity of DNMT5 domains is likely inherent to its functioning
498 and interaction with other epigenetic processes such as histone modifications and non-
499 coding RNA. In mammalian cells, TUDOR domain containing UHRF1 is known to
500 target DNMT1, the functional homologue of DNMT5, onto newly synthesized DNA
501 substrates during semi conservative DNA replication⁵². Furthermore, TUDOR domain
502 of UHRF1 was reported to play an important role in the recognition of histone H3K9
503 methylation^{53,54}. While UHRF1, DNMT1 and ATPase protein containing domains are
504 separate in animals, they form an unusual multifunctional domain protein in DNMT5 in
505 microeukaryotes. This domain architecture might be due to the compact genomes of
506 microalgae.

507 In our phylogeny study, the RID/DMTA and diatom DNMT4 enzymes are
508 related, as shown previously by Huff and Zilberman¹¹ and Punger and Li¹⁰. In our case,
509 because the analysis covers a large evolutionary distance, phylogenetic relationships
510 between DNMT families should be interpreted accordingly. Therefore, we cannot rule
511 out the possibility that diatoms and RID families are paraphyletic. The function of
512 DNMT4 or DNMT4-type enzymes in diatoms is unknown. Among the four diatoms with
513 a known methylation pattern on TEs, two are lacking DNMT4s (including *P.*
514 *tricornutum* presented in this study). The presence of chromodomains known to bind
515 histone post-translational modifications as in CMT enzymes⁵⁵ nonetheless suggests
516 that diatom DNMT4 might be functional as either a *de novo* or a maintenance enzyme.
517 The lack of chromatin-associated domains in DNMT3, DNMT6 and other DNMT4
518 proteins suggest that the link, if any, between DNA methylation and histone
519 modifications is more indirect than observed in plants and mammals and might require

520 the activity of accessory proteins like UHRF1-type⁵² or DNMT3-like⁵⁶ enzymes that
521 should be further investigated.

522 Examining the role of DNMT5a in the pennate diatom *P. tricornutum*, we found
523 that it is an orthologue of the single DNMT5a protein from *Cryptococcus neoformans*,
524 which is involved in the maintenance of DNA methylation^{11,15}. In that regard, our study
525 demonstrates that the loss of DNMT5a was sufficient alone to generate a global loss
526 of CG methylation in *P. tricornutum* similar to *Cryptococcus neoformans*¹¹. We further
527 confirm that TEs are major targets of DNA methylation in diatoms. Considering
528 cytosines with the highest levels of DNA methylation (>60%, at least 5X coverage), we
529 identified 10,349 methylated CGs for which 80% are found in TEs and their regulatory
530 regions (data not shown). In addition, DMR analysis identified regions essentially
531 composed of TEs that show extensive methylation in the reference strain. HypoDMRs
532 overlap with regions marked by H3K27me3 but also H3K9me3 which suggest that
533 histone post-translational modifications and DNA methylation cooperate to maintain
534 TE repression. Genes appear not to be the primary targets of DNA methylation. Only
535 51/9,416 genes are found within DMRs. Among them, 19 were upregulated in both KO
536 mutants. TE methylation is observed in other diatoms such as *F. cylindrus*¹¹ and *T.*
537 *pseudonana*¹¹ where the targeted TEs have low expression¹¹. However, those species
538 encode a different set of DNMTs compared to *P. tricornutum*. *T. pseudonana* appears
539 to lack DNMT5a and has a partial DNMT6 protein while *F. cylindrus* encodes all but
540 DNMT3 (Additional File 2: Table S3). It is possible that DNMTs show partial functional
541 redundancy in diatoms. In that regard, the DNMT5:KO lines presented in this study
542 could be used as a heterologous expression system to decipher the role of other
543 DNMTs in diatoms.

544 Compared to DNA methylation loss that is observed in different DNMT5:KO cell
545 lines (Additional File 1: Fig. S3), gene expression was more inconsistent between cell
546 lines, including when assessed by qPCR validation. We thus make the hypothesis that
547 gene expression is mainly cell line specific in DNMT5:KO lines. This divergence in
548 gene expression could be linked to the random insertions of plasmids generated by
549 biolistic transformation. Alternatively, *de novo* and likely random TE insertions upon
550 DNA methylation loss could generate gene expression divergence between cell lines
551 over time.

552 In our study, we found that 15% of TE-genes are upregulated in the DNMT5:KO
553 cell lines, less than observed in *Arabidopsis thaliana* where the loss of DDM1 (involved

554 in the maintenance of DNA methylation) caused the expression of about 40% of all TE-
555 genes⁵⁷. However, in *P. tricornutum* we found that overexpression and methylation
556 levels are particularly relevant for TEs that have been identified as full length potentially
557 still active LTR-copia elements. Interestingly, in *Arabidopsis thaliana*, the most mobile
558 TEs between different accessions are regulated by the MET2a protein, likely involved
559 in DNA methylation and repression⁵⁸. In addition, such TEs expansion associates with
560 null or loss of function alleles of MET2a⁵⁸. When comparing *P. tricornutum* and *T. pseudonana*
561 genomes, the CoDi2 and CoDi4 families are the main contributors of
562 retrotransposon expansion in *P. tricornutum*⁵⁹ although CoDi2 is only found in *P. tricornutum*.
563 We found such TEs to be overexpressed in response to DNA methylation
564 loss. Therefore, DNA methylation seems to be a genome integrity keeper in *P. tricornutum*.
565 Other smaller TEs in the form of TE-genes are also upregulated and may
566 retain some activity in *P. tricornutum*. Upregulation was also observed for TEs that
567 were not targets of DNA methylation in the reference strain but for which a subset was
568 nonetheless found within a 1 kb distance from hypoDMRs, suggesting that initial
569 repression is likely linked to DNA methylation spreading or proximity which was
570 reported in a previous work²⁷. Highly repetitive TE families are removed in our analysis
571 since only uniquely mapped reads were aligned. This is true for both transcriptomic
572 and bisulfite sequencing data. In addition, our transcriptomic analysis is only a
573 snapshot of all TEs overexpressed at a given time in *P. tricornutum* cell populations.
574 The loss of DNA methylation could trigger more misregulation of TEs in stress culture
575 conditions, as previously reported upon nitrogen depletion²⁷ and exposure to the toxic
576 reactive aldehyde⁵⁹. DNMT5 mutant cell lines are viable in standard culture conditions
577 used for *P. tricornutum* suggesting that co-occurring repressive histone marks reported
578 in previous studies might be compensating the loss of DNA methylation^{35,42}. This also
579 suggests that in optimal conditions, loss of DNA methylation is not associated with
580 drastic biological effects, supporting the lack of a phenotypic response which is
581 otherwise seen in stress conditions, typically slow growth, smaller cell size and an
582 atypical morphology. Our study provides the first insights into DNA methylation
583 regulation and its function in diatoms which ultimately will serve as a firm basis for
584 future studies in eukaryotes to better understand DNA methylation function and its
585 evolution.

586

587 **Acknowledgements**

588 We thank Catherine Cantrel from IBENS for media preparation. L.T. acknowledges
589 funds from the CNRS, the region of Pays de la Loire (ConnecTalent EPIALG project)
590 and Epicycle ANR project (ANR-19-CE20- 0028-02). C.B. acknowledges funding from
591 the ERC Advanced Awards Diatomite. F.Y. was supported by a PhD fellowship from
592 the Chinese Scholarship Council (CSC-201906310152).

593

594 **Author Contributions**

595 A.H. and L.T. conceived the study. A.H., F.R.J.V, O.A.M. and L.T. designed the study.
596 L.T. supervised and coordinated the study. A.H. performed the experiments. A.G. grew
597 the mutants and extracted RNA for validation experiments. F.Y. performed QPCR work
598 and gene validation analysis. O.A.M. performed and supervised A.H. for the
599 bioinformatic analysis of RNAseq, gene ontology and bisulfite seq data. A.H.
600 performed the DMR analysis under the supervision of O.A.M. F.R.J.V and
601 A.H. analyzed HMMER, DAMA/CLADE and eDAF data. All authors analyzed and
602 interpreted the data. A.H. and L.T. wrote the manuscript with input from all authors.

603 **Competing interests**

604 The authors declare no competing interests.

605

606 **Methods**

607 **Phylogenetic analysis of DNMTs in microeukaryotes**

608 The Phylogenetic analysis approach of DNMTs was conducted through three steps:

609 **1. HMMER and RBH analysis**

610 We performed an extensive scan of the MMETSP database, enriched with 7 diatom
611 transcriptomes and genomes from the top 20 most abundant diatoms found in *Tara*
612 Oceans database⁶⁰, using HMMER-search with the model PF00145 to fetch any
613 DNMT-like, including partial transcripts, sequence within microeukaryotes. We ran
614 HMMER in a non-stringent fashion to not miss positives DNMT sequences. We used
615 eDAF approach to filter the expected high number of false positives. It is worth noting
616 that we initially use HMMER for screening instead of the built-in module of eDAF due
617 to the time complexity of the latter for extensive searches (tens to hundreds of times
618 slower than HMMER). Reciprocal BLAST best hit analysis was performed as
619 previously described⁶¹. The DNMT3 (*Phatr3_J47136*), DNMT4 (*Thaps3_11011*),
620 DNMT5 (*Phatr3_EG02369*) and DNMT6 (*Phatr3_J47357*) orthologues found in *P.*

621 *tricornutum* or *T. pseudonana* (for DNMT4) were blasted on a phylogenetically
622 optimized database that include MMETSP transcriptomes. Upon reciprocal BLAST,
623 putative DNMT sequence hits giving back the corresponding enzyme (DNMT3,
624 DNMT4, DNMT5 or DNMT6) at the threshold of e-value of 1×10^{-5} in the corresponding
625 diatom were retained. Candidate enzymes were then analyzed using eDAF.

626 **2. eDAF-guided domain architecture analysis**

627 enhanced Domain Architecture Framework (eDAF) is a four module computational tool
628 for gene prediction, gene ontology and functional domain predictions³⁵. As previously
629 described for Polycomb and Trithorax enzymes³⁵, candidate DNMTs identified by RBH
630 and HMMER-search were analyzed using the DAMA-CLADE guided built-in functional
631 domain architecture. The domain architecture of representative enzymes used in this
632 study can be found in Additional File 2: Table S4.

633 **3. Phylogenetic tree analysis**

634 The DNMT domain of candidate enzymes were aligned using ClustalΩ⁶² (HHalign
635 algorithm). The alignment was manually curated and trimmed using trimAL (removing
636 >25% gap column) to align corresponding DNMT motifs in all gene families. A
637 convergent phylogenetic tree was then generated using the online CIPRES Science
638 gateway program⁶³ using MrBAYES built-in algorithm. Default parameters were used
639 with the following specifications for calculation of the posterior probability of partition:
640 sumt.burninfraction=0.5, sumt.burningfraction=0.5, 10000000 generations, sampling
641 each 100. We also used two different models: Estimating the Fixed Rate and GTR.

642 **Cell cultures**

643 Axenic *P. tricornutum* CCMP2561 clone Pt18.6 cultures were obtained from the culture
644 collection of the Provasoli-Guillard National Center for Culture of Marine Phytoplankton
645 (Bigelow Laboratory for Ocean Sciences, USA.). Cultures were grown in autoclaved
646 and filtered (0.22 µM) Enhanced Sea Artificial Water (ESAW -
647 https://biocyclopedia.com/index/algae/algal_culturing/esaw_medium_composition.php)
648 medium supplemented with f/2 nutrients and vitamins without silica under constant
649 shaking (100rpm). Cultures were maintained in flasks at exponential state in a
650 controlled growth chamber at 19°C under cool white fluorescent lights at 100 µE m⁻²
651 s⁻¹ with a 12h photoperiod. For RNA sequencing and bisulfite experiments, WT and
652 DNMT5 mutant cultures were seeded in duplicate at 10.000 cells/ml and grown side
653 by side in 250ml flasks until early-exponential at 1.000.000 cells/ml. Culture growth

654 was followed using a hematocytometer (Fisher Scientific, Pittsburgh, PA, USA). Pellets
655 were collected by centrifugation (4000rpm) washed twice with marine PBS
656 (<http://cshprotocols.cshlp.org/content/2006/1/pdb.rec8303>) and flash frozen in liquid
657 nitrogen. Cell pellets were kept at -80°C until use. For bisulfite sequencing, technical
658 duplicates were pooled to get sufficient materials.

659 **CRISPR/Cas9 mediated gene extinction**

660 The CRISPR/Cas9 knockouts were performed as previously described ⁶⁴. Our strategy
661 consisted in the generation of short deletions and insertions to disrupt the open reading
662 frame of putative DNMTs of *P. tricornutum*. We introduced by biolistic the guide RNAs
663 independently of the Cas9 and ShBle plasmids, conferring resistance to Phleomycin,
664 into the reference strain Pt18.6 (referred hereafter as 'reference line' or 'wild-type'-
665 WT). Briefly, specific target guide RNAs were designed in the first exon of
666 Phatr3_EG02369 (DNMT5), Phatr3_J47357 (DNMT6) and Phatr3_J36137 (DNMT3)
667 using the PHYTO/CRISPR-EX ⁶⁵ software and cloned into the pU6::AOX-sgRNA
668 plasmid by PCR amplification. For PCR amplification, plasmid sequences were added
669 in 3' of the guide RNA sequence (minus -NGG) which are used in a PCR reaction with
670 the template pU6::AOX-sgRNA. Forward primer - sgRNA seq +
671 GTTTTAGAGCTAGAAATAGC. Reverse primer - sequence to add in 3' reverse
672 sgRNA seq + CGACTTTGAAGGTGTTTTG. This will amplify a new pU6::AOX-
673 (your_sgRNA). The PCR product is digested by the enzyme DPN1 (NEB) in order to
674 remove the template plasmid and cloned in TOPO10 *E. coli*. The sgRNA plasmid, the
675 pDEST-hCas9-HA and the ShBLE Phleomycin resistance gene cloned into the plasmid
676 pPHAT-eGFP were co-transformed by biolistic in the Pt18.6 'Wild Type' strain as
677 described in ⁶⁴. We also generated a line that was transformed with pPHAT-eGFP and
678 pDEST-hCas9-HA but no guide RNAs. This line is referred as the Cas9:Mock line.

679 **RNA and DNA extraction**

680 Total RNA extraction was performed by classical TRIZOL/Chloroform isolations and
681 precipitation by isopropanol. Frozen cell pellets were extracted at a time in a series of
682 3 technical extraction/duplicates and pooled. RNA was DNase treated using DNase I
683 (ThermoFisher) as per manufacturer's instructions. DNA extraction was performed
684 using the Invitrogen™ Easy-DNA™ gDNA Purification Kit following 'Protocol #3'
685 instructions provided by the manufacturer. Extracted nucleic acids were measured
686 using QUBIT fluorometer and NANODROP spectrometer. RNA and gDNA Integrity
687 were controlled by electrophoresis on 1% agarose gels.

688 **RT-qPCR analysis**

689 qPCR primers were designed using the online PRIMER3 program v0.4.0 defining 110-
690 150 amplicon size and annealing temperature between 58°C and 62°C. Primer
691 specificity was checked by BLAST on *P. tricornutum* genome at ENSEMBL. For cDNA
692 synthesis, 1µg of total RNA was reverse transcribed using the SuperScript™ III First-
693 Strand (Invitrogen) protocol. For quantitative reverse transcription polymerase chain
694 reaction (RT-qPCR) analysis, cDNA was amplified using SYBR Premix ExTaq (Takara,
695 Madison, WI, USA) according to manufacturer's instructions. CT values for genes of
696 interest were generated on a Roche lightcycler® 480 qpcr system. CT values were
697 normalized on housekeeping genes using the deltaCT method. Normalized CT values
698 for amplifications using multiple couple of primers targeting several cDNA regions of
699 the genes of interest were then averaged and used as RNA levels proxies.

700 **Dot blot**

701 gDNA samples were boiled at 95°C for 10 min for denaturation. Samples were
702 immediately placed on ice for 5 min, and 250-500 ng were loaded on regular
703 nitrocellulose membranes. DNA was then autocrosslinked in a UVC 500 crosslinker –
704 2 times at 1200uj (*100). The membranes were blocked for 1 hr in 5% PBST-BSA.
705 Membranes were probed for 1 hr at room temperature or overnight at 4°C with 1:1000
706 dilution of 5mC antibody (OptimAbtm Anti-5-Methylcytosine – BY-MECY 100). 5mC
707 signals were revealed using 1:5000 dilution of HRP conjugated antirabbit IgG
708 secondary antibody for 1 hr at room temperature followed by chemo luminescence.
709 Loading was measured using methylene blue staining.

710 **RNA and Bisulfite sequencing**

711 RNA libraries were prepared by the FASTERIS Company (<https://www.fasteris.com>).
712 Total RNA was polyA purified and libraries were prepared for illumina NextSeq
713 sequencing technologies. For RNAseq analysis, two biological replicates per mutant
714 were used (M23 and M25). In addition, two biological replicates of a Pt18.6 line was
715 sequenced in the same run as a control (total of 6 samples). Bisulfite libraries and
716 treatments were performed by the FASTERIS Company and DNA was sequenced on
717 an Illumina NextSeq instrument. 150bp Pair-end reads were generated with 30X
718 coverage. A new 5mC map was also generated in the reference Pt18.6 line as a
719 control.

720 **RNAseq analysis**

721 150bp pair-end sequenced reads were subjected to quality control with FastQC
722 (<https://www.bioinformatics.babraham.ac.uk/projects/fastqc>). Then, the reads were
723 aligned on the reference genome of *P. tricornutum* (Phatr3)⁴⁴ using STAR (v2.5.3a).
724 Gene expression levels were quantified using HTseq v0.7.2. Differentially expressed
725 genes were analyzed using DESeq2 v1.19.37 with the following generalized linear
726 model: ~mutation. FDR values are corrected p.values using the Benjamin and
727 Hochberg method. Genes are designed significant (DEGs) if the $|\log_{2}FC| > 1$ and the
728 FDR < 0.05 . GO enrichments were calculated using the overrepresentation Fisher's
729 exact test described in topGO v2.44.0⁶⁶. For each analysis, appropriate DEGs have
730 been used as input and a GO theme is considered as significant if the p.value < 0.05 .

731

732 **Bisulfite sequencing analysis**

733 Bisulfite analysis was performed using Bismark-bowtie 2
734 (<https://www.bioinformatics.babraham.ac.uk/projects/bismark/>). We used the default
735 Bowtie2 implementation of bismark with the specifications that only uniquely mapped
736 reads should be aligned. All alignments were performed with high stringency allowing
737 for only one base mismatch ($n = 1$). We also clearly specified that no discordant pairs
738 of the pair-end reads should be aligned. DNA methylation in the CG, CHG and CHH
739 contexts was calculated by dividing the total number of aligned methylated reads by
740 the total number of methylated plus un-methylated reads.

741 **DMR calling**

742 Differentially methylated regions were called using the DMRcaller R package v1.22.0
743⁴³. Given the low level of correlation of DNA methylation observed in *P. tricornutum*
744^{11,27} and sequencing coverage in all three cell lines, only cytosines with coverage $\geq 5X$
745 in all three lines were kept for further analysis and the bins strategy was favored over
746 other built-in DMRcaller tools. DMRs were defined as 100bp regions with at least an
747 average 20% loss/gain of DNA methylation in either one of the DNMT5:KOs compared
748 to the reference strain. The 'Score test' method was used to calculate statistical
749 significance and threshold was set at p.value < 0.01 . In addition, to distinguish isolated
750 differentially methylated cytosines from regions with significant loss of DNA
751 methylation, an hypoDMR must contain at least methylated 2 CpG in the reference
752 strain.

753 **Overlap with histone modifications and genomic annotations.**

754 Analysis on bed files were performed using bedtools v2.27.1.⁶⁷ Bedtools intersect with
755 default parameters was used to calculate overlap regions of DMRs with genes and TE-
756 genes. Bedtools window has been used to compute the 500 bp and 1kb upstream and
757 downstream near regions between DMRs, genes and TE-genes.

758 Percentage overlaps between DMRs as well as the overlap of gene and TEs
759 coordinates with histone modifications and DMRs were calculated using the
760 genomation R package v1.22.0⁶⁸ and the ‘annotateWithFeature’ and ‘getMembers’
761 functions. For RNAseq analysis, we analyzed the expression of TE-genes as
762 previously defined⁴⁴. To define TE-genes in DMRs we crosschecked overlapping TE-
763 genes annotations with *bona fide* TEs in DMRs using ‘annotateWithFeature’ function.
764 UpSet plots were computed using UpSetR v1.4.0.⁶⁹ Heatmaps were produced using
765 the R package ComplexHeatmap⁷⁰ (v2.8.0). All R plots were obtained using R version
766 4.0.3. Sankey diagram was produced with the R package highcharter (v0.9.4)(
767 reference <https://jkunst.com/highcharter/authors.html>). TEs that mapped to less than 3
768 members of a TE family were discarded.

769 **Data availability**

770 The raw data have been deposited at Gene Expression Omnibus GEO
771 (<https://www.ncbi.nlm.nih.gov/geo/query/acc.cgi?acc=GSE186857>). Bisulfite
772 sequencing raw data and bigwig files showing methylation rates (#methylated C/#total
773 number of C) in the context of CHH, CHG and CpG, where H: is A, C or T in the WT,
774 M23 and M25 are under the accession number GSE186855. The raw RNA sequencing
775 data and the TPM counting table are under accession GSE186856. Raw data can be
776 accessed using the following reviewer token: ehctuyaedlojpcj. The bigwig files and *P.*
777 *tricornutum* genome reference file can be uploaded from this link for IGV visualization
778 ([https://1drv.ms/f/s!BOcWdlxP0cmH5jbu3_kPAPd3NwG-
779 ?e=LQ6sKrjDUUu0_FQe_Z19Qg&at=9](https://1drv.ms/f/s!BOcWdlxP0cmH5jbu3_kPAPd3NwG-?e=LQ6sKrjDUUu0_FQe_Z19Qg&at=9)).

780 All the code that has been used to generate the results in this paper is available from
781 the lead contact upon request.

782

783 **References**

784

785 1. Kato, M., Miura, A., Bender, J., Jacobsen, S. E. & Kakutani, T. Role of CG and

786 non-CG methylation in immobilization of transposons in *Arabidopsis*. *Curr. Biol.*
787 (2003) doi:10.1016/S0960-9822(03)00106-4.

788 2. Zilberman, D. The evolving functions of DNA methylation. *Current Opinion in*
789 *Plant Biology* (2008) doi:10.1016/j.pbi.2008.07.004.

790 3. Barlow, D. P. & Bartolomei, M. S. Genomic imprinting in mammals. *Cold Spring*
791 *Harb. Perspect. Biol.* (2014) doi:10.1101/csfperspect.a018382.

792 4. Galupa, R. & Heard, E. X-Chromosome Inactivation: A Crossroads Between
793 Chromosome Architecture and Gene Regulation. *Annu. Rev. Genet.* (2018)
794 doi:10.1146/annurev-genet-120116-024611.

795 5. Bestor, T. H. DNA methylation: evolution of a bacterial immune function into a
796 regulator of gene expression and genome structure in higher eukaryotes.
797 *Philosophical transactions of the Royal Society of London. Series B, Biological*
798 *sciences* (1990) doi:10.1098/rstb.1990.0002.

799 6. Kumar, S. *et al.* The DNA (cytosine-5) methyltransferases. *Nucleic Acids*
800 *Research* (1994) doi:10.1093/nar/22.1.1.

801 7. Cheng, X., Kumar, S., Klimasauskas, S. & Roberts, R. J. Crystal structure of
802 the Hhal DNA methyltransferase. in *Cold Spring Harbor Symposia on*
803 *Quantitative Biology* (1993). doi:10.1101/SQB.1993.058.01.039.

804 8. Zemach, A. & Zilberman, D. Evolution of eukaryotic DNA methylation and the
805 pursuit of safer sex. *Current Biology* (2010) doi:10.1016/j.cub.2010.07.007.

806 9. Zemach, A., McDaniel, I. E., Silva, P. & Zilberman, D. Genome-wide
807 evolutionary analysis of eukaryotic DNA methylation. *Science* (80-.). (2010)
808 doi:10.1126/science.1186366.

809 10. Ponger, L. & Li, W. H. Evolutionary diversification of DNA methyltransferases in
810 eukaryotic genomes. *Mol. Biol. Evol.* (2005) doi:10.1093/molbev/msi098.

811 11. Huff, J. T. & Zilberman, D. Dnmt1-independent CG methylation contributes to
812 nucleosome positioning in diverse eukaryotes. *Cell* (2014)
813 doi:10.1016/j.cell.2014.01.029.

814 12. Greenberg, M. V. C. & Bourc'his, D. The diverse roles of DNA methylation in
815 mammalian development and disease. *Nature Reviews Molecular Cell Biology*
816 (2019) doi:10.1038/s41580-019-0159-6.

817 13. Seritrakul, P. & Gross, J. M. Expression of the De Novo DNA
818 Methyltransferases (dnmt3-dnmt8) During Zebrafish Lens Development.
819 doi:10.1002/dvdy.24077.

820 14. Kouzminova, E. & Selker, E. U. Dim-2 encodes a DNA methyltransferase
821 responsible for all known cytosine methylation in *Neurospora*. *EMBO J.* (2001)
822 doi:10.1093/emboj/20.15.4309.

823 15. Dumesic, P. A., Stoddard, C. I., Catania, S., Narlikar, G. J. & Madhani, H. D.
824 ATP Hydrolysis by the SNF2 Domain of Dnmt5 Is Coupled to Both Specific
825 Recognition and Modification of Hemimethylated DNA. *Mol. Cell* (2020)
826 doi:10.1016/j.molcel.2020.04.029.

827 16. Gladyshev, E. Repeat-Induced Point Mutation and Other Genome Defense
828 Mechanisms in Fungi. *Microbiol. Spectr.* (2017)
829 doi:10.1128/microbiolspec.funk-0042-2017.

830 17. Galagan, J. E. & Selker, E. U. RIP: The evolutionary cost of genome defense.
831 *Trends in Genetics* (2004) doi:10.1016/j.tig.2004.07.007.

832 18. Yang, K. *et al.* The DmtA methyltransferase contributes to *Aspergillus flavus*
833 conidiation, sclerotial production, aflatoxin biosynthesis and virulence. *Sci.
834 Rep.* (2016) doi:10.1101/srep23259.

835 19. Malagnac, F. *et al.* A gene essential for de novo methylation and development
836 in *ascobolus* reveals a novel type of eukaryotic DNA methyltransferase
837 structure. *Cell* (1997) doi:10.1016/S0092-8674(00)80410-9.

838 20. Bewick, A. J., Vogel, K. J., Moore, A. J. & Schmitz, R. J. Evolution of DNA
839 methylation across insects. *Mol. Biol. Evol.* (2017)
840 doi:10.1093/molbev/msw264.

841 21. Feng, S. *et al.* Conservation and divergence of methylation patterning in plants
842 and animals. *Proc. Natl. Acad. Sci. U. S. A.* (2010)
843 doi:10.1073/pnas.1002720107.

844 22. Vanyushin, B. F. & Ashapkin, V. V. *DNA methylation in plants. DNA
845 Methylation in Plants* (2011). doi:10.1146/annurev.arplant.49.1.223.

846 23. Zhong, X. *et al.* Molecular mechanism of action of plant DRM de novo DNA
847 methyltransferases. *Cell* (2014) doi:10.1016/j.cell.2014.03.056.

848 24. Jeltsch, A. *et al.* Mechanism and biological role of Dnmt2 in Nucleic Acid
849 Methylation. *RNA Biology* (2017) doi:10.1080/15476286.2016.1191737.

850 25. Goll, M. G. *et al.* Methylation of tRNAAsp by the DNA methyltransferase
851 homolog Dnmt2. *Science* **311**, 395–398 (2006).

852 26. De Mendoza, A. *et al.* Recurrent acquisition of cytosine methyltransferases into
853 eukaryotic retrotransposons. *Nat. Commun.* (2018) doi:10.1038/s41467-018-

854 03724-9.

855 27. Veluchamy, A. *et al.* Insights into the role of DNA methylation in diatoms by
856 genome-wide profiling in *Phaeodactylum tricornutum*. *Nat. Commun.* (2013)
857 doi:10.1038/ncomms3091.

858 28. Fan, X. *et al.* Single-base methylome profiling of the giant kelp *Saccharina*
859 *japonica* reveals significant differences in DNA methylation to microalgae and
860 plants. *New Phytol.* (2020) doi:10.1111/nph.16125.

861 29. Armbrust, E. V. The life of diatoms in the world's oceans. *Nature* (2009)
862 doi:10.1038/nature08057.

863 30. Malviya, S. *et al.* Insights into global diatom distribution and diversity in the
864 world's ocean. *Proc. Natl. Acad. Sci. U. S. A.* (2016)
865 doi:10.1073/pnas.1509523113.

866 31. Traller, J. C. *et al.* Genome and methylome of the oleaginous diatom *Cyclotella*
867 *cryptica* reveal genetic flexibility toward a high lipid phenotype. *Biotechnol.*
868 *Biofuels* (2016) doi:10.1186/s13068-016-0670-3.

869 32. Lister, R. *et al.* Human DNA methylomes at base resolution show widespread
870 epigenomic differences. *Nature* (2009) doi:10.1038/nature08514.

871 33. Maumus, F., Rabinowicz, P., Bowler, C. & Rivarola, M. Stemming Epigenetics
872 in Marine Stramenopiles. *Curr. Genomics* (2011)
873 doi:10.2174/138920211796429727.

874 34. Keeling, P. J. *et al.* The Marine Microbial Eukaryote Transcriptome Sequencing
875 Project (MMETSP): Illuminating the Functional Diversity of Eukaryotic Life in
876 the Oceans through Transcriptome Sequencing. *PLoS Biol.* (2014)
877 doi:10.1371/journal.pbio.1001889.

878 35. Zhao, X. *et al.* Probing the Diversity of Polycomb and Trithorax Proteins in
879 Cultured and Environmentally Sampled Microalgae. *Front. Mar. Sci.* (2020)
880 doi:10.3389/fmars.2020.00189.

881 36. Remmert, M., Biegert, A., Hauser, A. & Söding, J. HHblits: lightning-fast
882 iterative protein sequence searching by HMM-HMM alignment. *Nat. Methods*
883 2011 92 9, 173–175 (2011).

884 37. Simões, T. R., Vernygora, O., Caldwell, M. W. & Pierce, S. E.
885 Megaevolutionary dynamics and the timing of evolutionary innovation in
886 reptiles. *Nat. Commun.* 2020 111 11, 1–14 (2020).

887 38. Czech, L., Huerta-Cepas, J. & Stamatakis, A. A Critical Review on the Use of

888 Support Values in Tree Viewers and Bioinformatics Toolkits. *Mol. Biol. Evol.*
889 **34**, 1535–1542 (2017).

890 39. Kelk, S. Phylogenetic Networks: Concepts, Algorithms and Applications. *Syst.*
891 *Biol.* **61**, 174–175 (2012).

892 40. Bewick, A. J. *et al.* Diversity of cytosine methylation across the fungal tree of
893 life. *Nat. Ecol. Evol.* (2019) doi:10.1038/s41559-019-0810-9.

894 41. Jurkowska, R. Z., Jurkowski, T. P. & Jeltsch, A. Structure and Function of
895 Mammalian DNA Methyltransferases. *ChemBioChem* (2011)
896 doi:10.1002/cbic.201000195.

897 42. Veluchamy, A. *et al.* An integrative analysis of post-translational histone
898 modifications in the marine diatom *Phaeodactylum tricornutum*. *Genome Biol.*
899 (2015) doi:10.1186/s13059-015-0671-8.

900 43. Catoni, M., Tsang, J. M. F., Greco, A. P. & Zabet, N. R. DMRcaller: A versatile
901 R/Bioconductor package for detection and visualization of differentially
902 methylated regions in CpG and non-CpG contexts. *Nucleic Acids Res.* (2018)
903 doi:10.1093/nar/gky602.

904 44. Rastogi, A. *et al.* Integrative analysis of large scale transcriptome data draws a
905 comprehensive landscape of *Phaeodactylum tricornutum* genome and
906 evolutionary origin of diatoms. *Sci. Rep.* (2018) doi:10.1038/s41598-018-
907 23106-x.

908 45. Filloromo, G. V., Curtis, B. A., Blanche, E. & Archibald, J. M. Re-examination of
909 two diatom reference genomes using long-read sequencing. *BMC Genomics*
910 **22**, 1–25 (2021).

911 46. Cuypers, B. *et al.* The Absence of C-5 DNA Methylation in *Leishmania*
912 *donovani* Allows DNA Enrichment from Complex Samples. *Microorganisms* **8**,
913 1–18 (2020).

914 47. Grüne, T. *et al.* Crystal structure and functional analysis of a nucleosome
915 recognition module of the remodeling factor ISWI. *Mol. Cell* (2003)
916 doi:10.1016/S1097-2765(03)00273-9.

917 48. Lu, R. & Wang, G. G. Tudor: A versatile family of histone methylation ‘readers’.
918 *Trends in Biochemical Sciences* (2013) doi:10.1016/j.tibs.2013.08.002.

919 49. Pek, J. W., Anand, A. & Kai, T. Tudor domain proteins in development. *Dev.*
920 (2012) doi:10.1242/dev.073304.

921 50. Tóth, K. F., Pezic, D., Stuwe, E. & Webster, A. The pirna pathway guards the

922 germline genome against transposable elements. in *Advances in Experimental*
923 *Medicine and Biology* (2016). doi:10.1007/978-94-017-7417-8_4.

924 51. Catania, S. *et al.* Evolutionary Persistence of DNA Methylation for Millions of
925 Years after Ancient Loss of a De Novo Methyltransferase. *Cell* **180**, 816
926 (2020).

927 52. Bostick, M. *et al.* UHRF1 plays a role in maintaining DNA methylation in
928 mammalian cells. *Science* (80-.). (2007) doi:10.1126/science.1147939.

929 53. Nady, N. *et al.* Recognition of multivalent histone states associated with
930 heterochromatin by UHRF1 protein. *J. Biol. Chem.* **286**, 24300–24311 (2011).

931 54. Rottach, A. *et al.* The multi-domain protein Np95 connects DNA methylation
932 and histone modification. *Nucleic Acids Res.* **38**, 1796 (2010).

933 55. Tajul-Arifin, K. *et al.* Identification and Analysis of Chromodomain-Containing
934 Proteins Encoded in the Mouse Transcriptome. *Genome Res.* **13**, 1416–1429
935 (2003).

936 56. Ooi, S. K. T. *et al.* DNMT3L connects unmethylated lysine 4 of histone H3 to de
937 novo methylation of DNA. *Nature* (2007) doi:10.1038/nature05987.

938 57. Osakabe, A. *et al.* The chromatin remodeler DDM1 prevents transposon
939 mobility through deposition of histone variant H2A.W. *Nat. Cell Biol.* **23**, 391–
940 400 (2021).

941 58. Quadrana, L. *et al.* The *Arabidopsis thaliana* mobilome and its impact at the
942 species level. *eLife* **5**, (2016).

943 59. Maumus, F. *et al.* Potential impact of stress activated retrotransposons on
944 genome evolution in a marine diatom. *BMC Genomics* (2009)
945 doi:10.1186/1471-2164-10-624.

946 60. Dorrell, R. G. *et al.* Phylogenomic fingerprinting of tempo and functions of
947 horizontal gene transfer within ochrophytes. doi:10.1073/pnas.2009974118/-
948 /DCSupplemental.

949 61. Dorrell, R. G. *et al.* Chimeric origins of ochrophytes and haptophytes revealed
950 through an ancient plastid proteome. *eLife* (2017) doi:10.7554/eLife.23717.

951 62. Madeira, F. *et al.* The EMBL-EBI search and sequence analysis tools APIs in
952 2019. *Nucleic Acids Res.* (2019) doi:10.1093/nar/gkz268.

953 63. Miller, M. A., Pfeiffer, W. & Schwartz, T. Creating the CIPRES Science
954 Gateway for inference of large phylogenetic trees. in *2010 Gateway Computing*
955 *Environments Workshop, GCE 2010* (2010). doi:10.1109/GCE.2010.5676129.

956 64. Nymark, M., Sharma, A. K., Sparstad, T., Bones, A. M. & Winge, P. A
957 CRISPR/Cas9 system adapted for gene editing in marine algae. *Sci. Rep.*
958 (2016) doi:10.1038/srep24951.

959 65. Rastogi, A., Murik, O., Bowler, C. & Tirichine, L. PhytoCRISP-Ex: A web-based
960 and stand-alone application to find specific target sequences for CRISPR/CAS
961 editing. *BMC Bioinformatics* (2016) doi:10.1186/s12859-016-1143-1.

962 66. Alexa, A. & Maintainer, J. R. Package ‘topGO’ Type Package Title Enrichment
963 Analysis for Gene Ontology. (2022).

964 67. BEDTools: a flexible suite of utilities for comparing genomic features |
965 Genomics Gateway. <http://bioscholar.com/genomics/bedtools-a-flexible-suite-of-utilities-for-comparing-genomic-features/>.

966 68. Akalin, A., Franke, V., Vlahoviček, K., Mason, C. E. & Schübeler, D.
967 Genomation: A toolkit to summarize, annotate and visualize genomic intervals.
968 *Bioinformatics* (2015) doi:10.1093/bioinformatics/btu775.

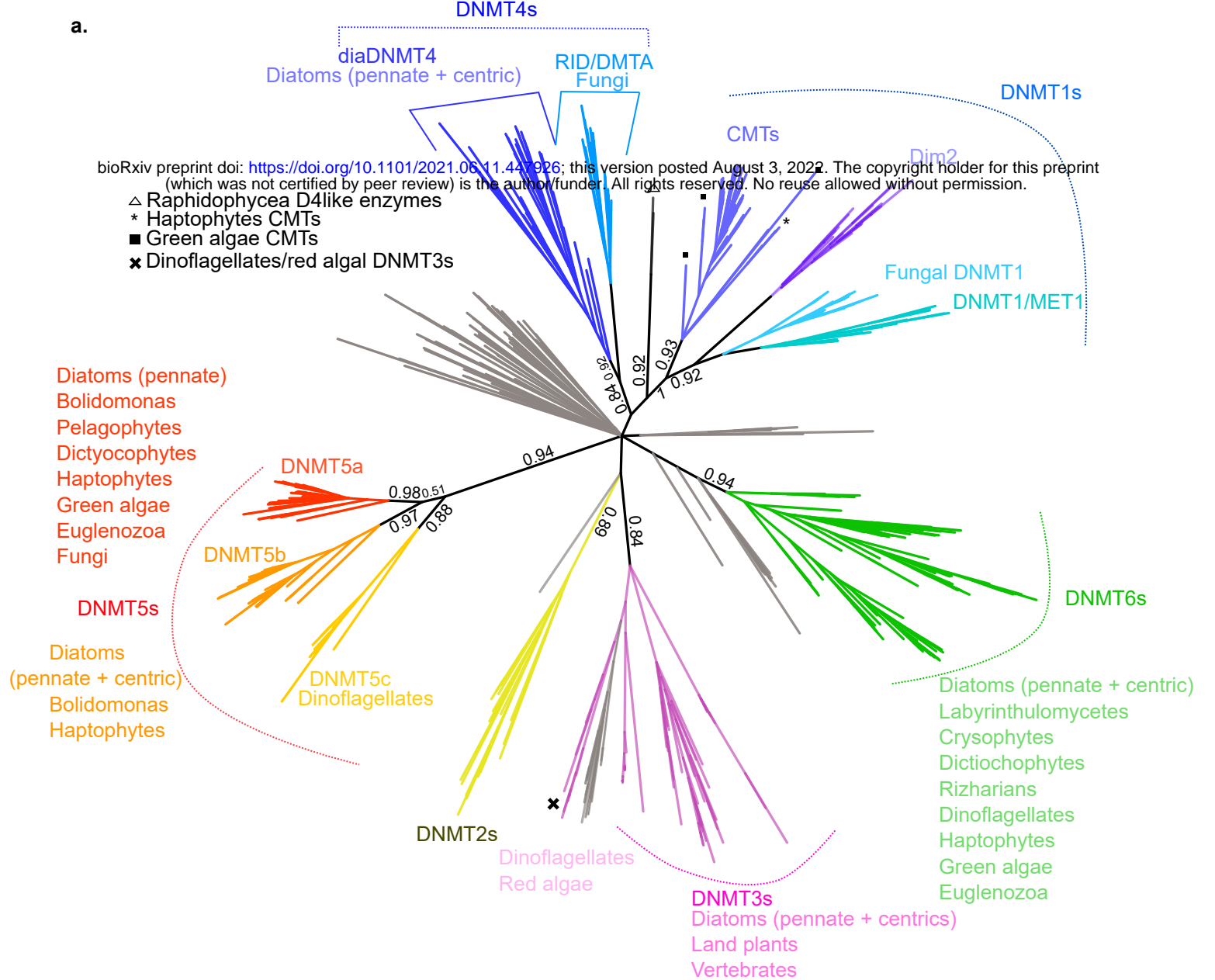
969 69. Lex, A. Sets and intersections. *Nat. Methods* **11**, 779 (2014).

970 70. Gu, Z., Eils, R. & Schlesner, M. Complex heatmaps reveal patterns and
971 correlations in multidimensional genomic data. *Bioinformatics* **32**, 2847–2849
972 (2016).

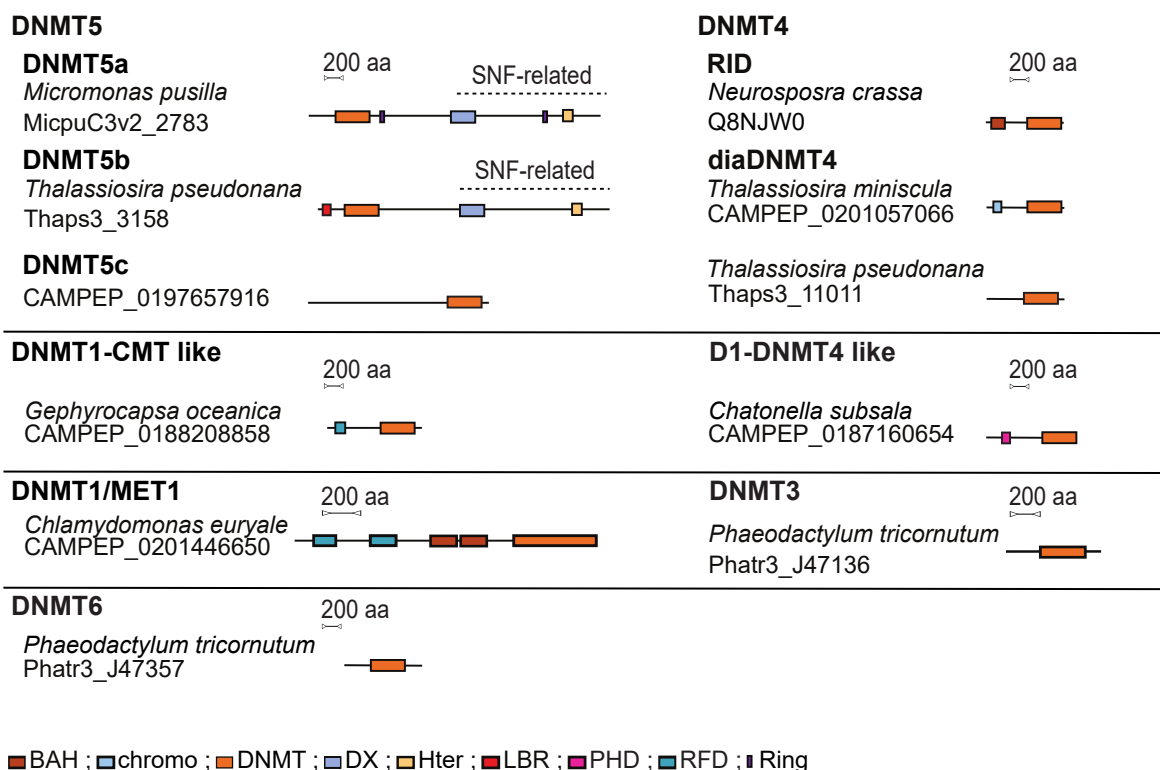
973

974

a.



b.

**Fig. 1**

Phylogenetic analysis of DNMTs from MMETSP

a. Convergent phylogenetic tree of DNMT domains from the MMETSP and reference genome databases. The sequences selected were from microeukaryotes. Numbers represent MrBAYES posterior probabilities. Grey branches represent bacterial and viral DCM enzymes. We indicate the main lineages found within each gene family using their corresponding colours next to the tree. b. Schematic representation of the DAMA/CLADE structure of representative DNMT enzymes. DNMT: DNA methyltransferase; RING: Ring zinc finger domain; DX: Dead box helicase; Hter: C-terminus-Helicase; LBR: Laminin B receptor; RFD: Replication Foci Domain; BAH: Bromo-Adjacent Homology; Chromo: Chromodomain; PHD: Plant HomeoDomain.

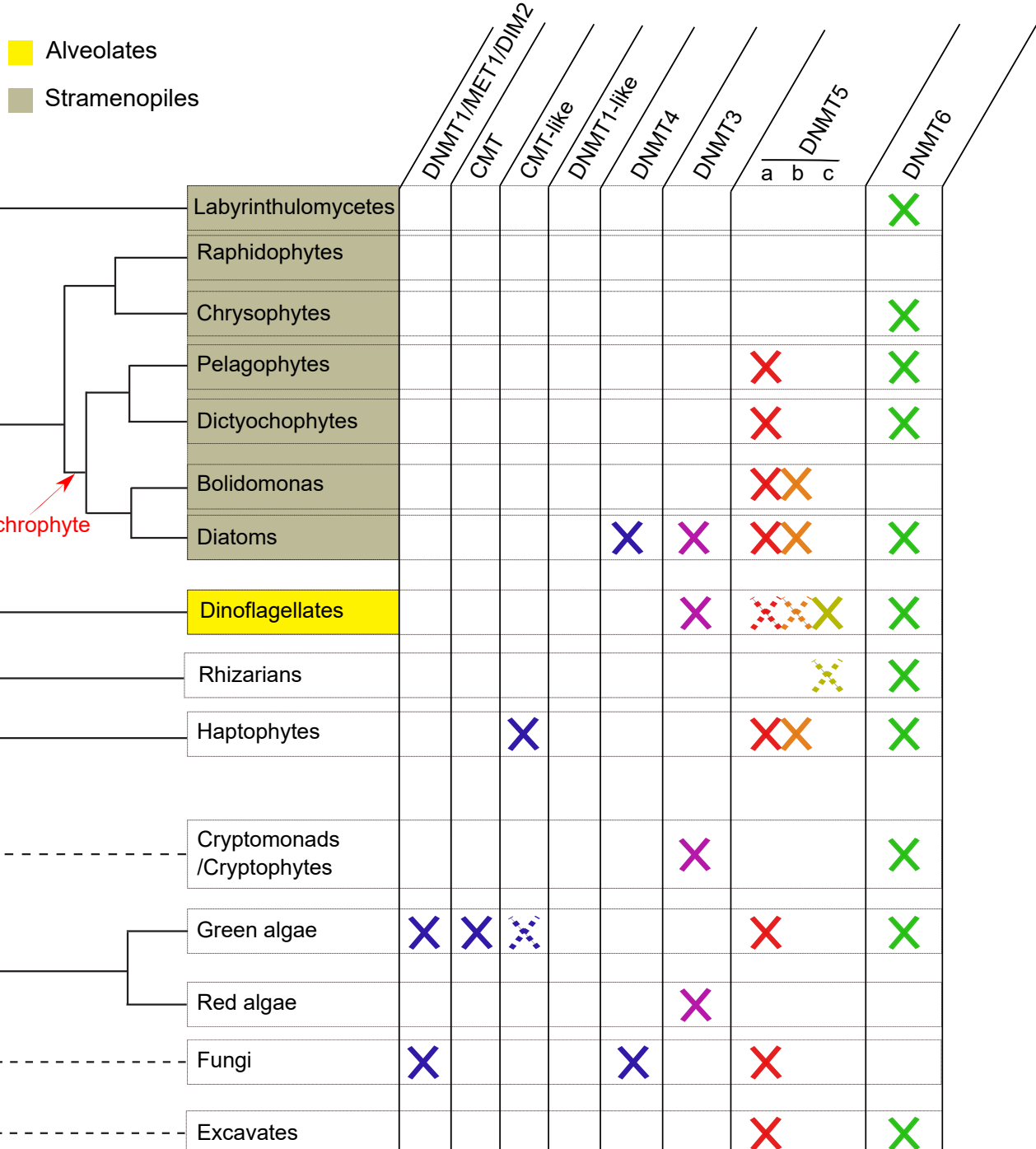


Fig. 2

Summary of DNMT family lineages found in microeukaryotes

Full crosses report the presence of a given gene family within lineages. Dashed lines and crosses indicate the uncertainty in the eukaryotic phylogeny as well as low support presence of a given DNMT family within lineages. Fungi that share DNMT families with other eukaryotes presented in this study are shown for comparison purposes. SAR: Stramenopile Alveolate Rhizaria lineage. Ochrophyte are secondary endosymbiont, photosynthetic lineages of stramenopiles.

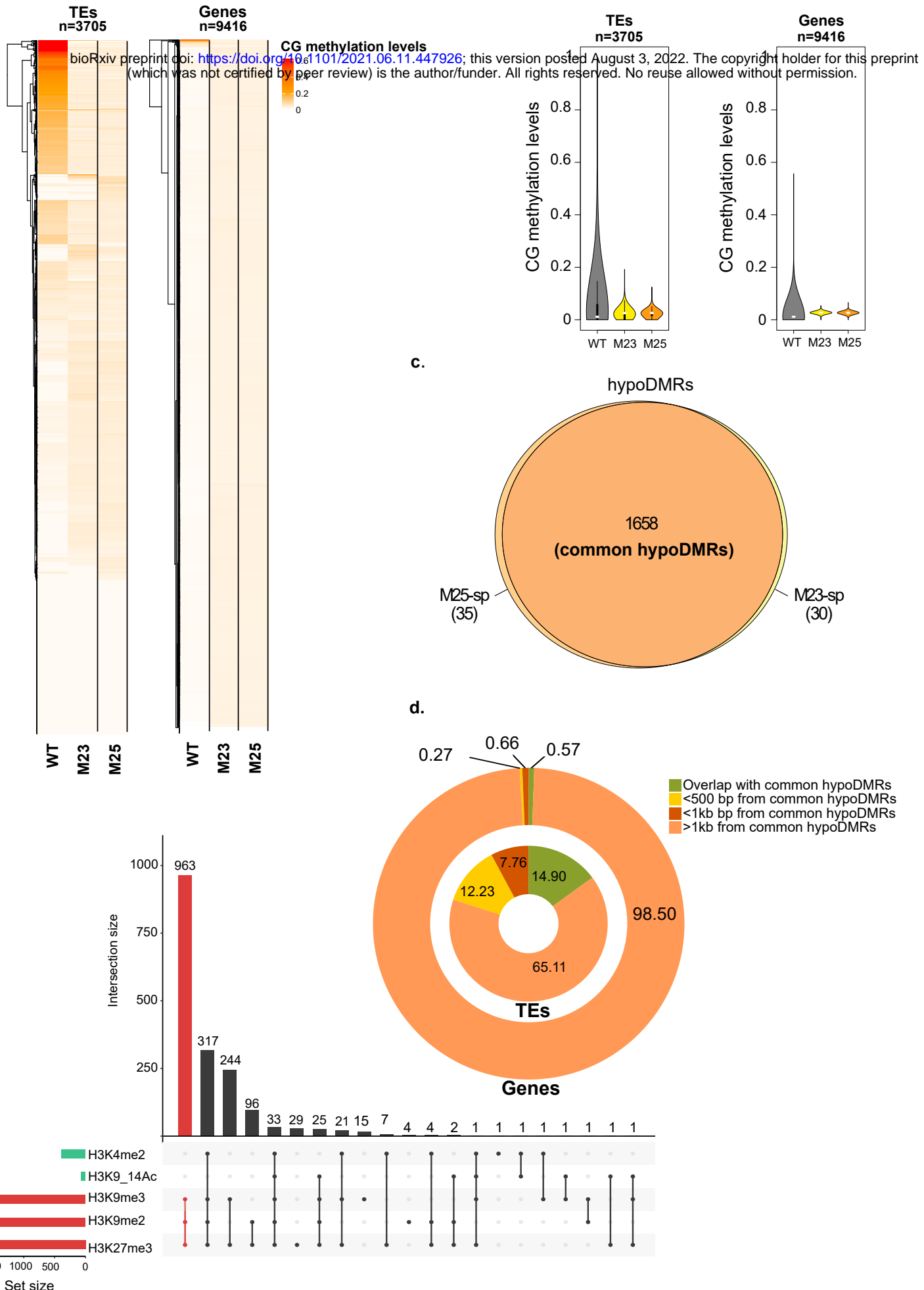
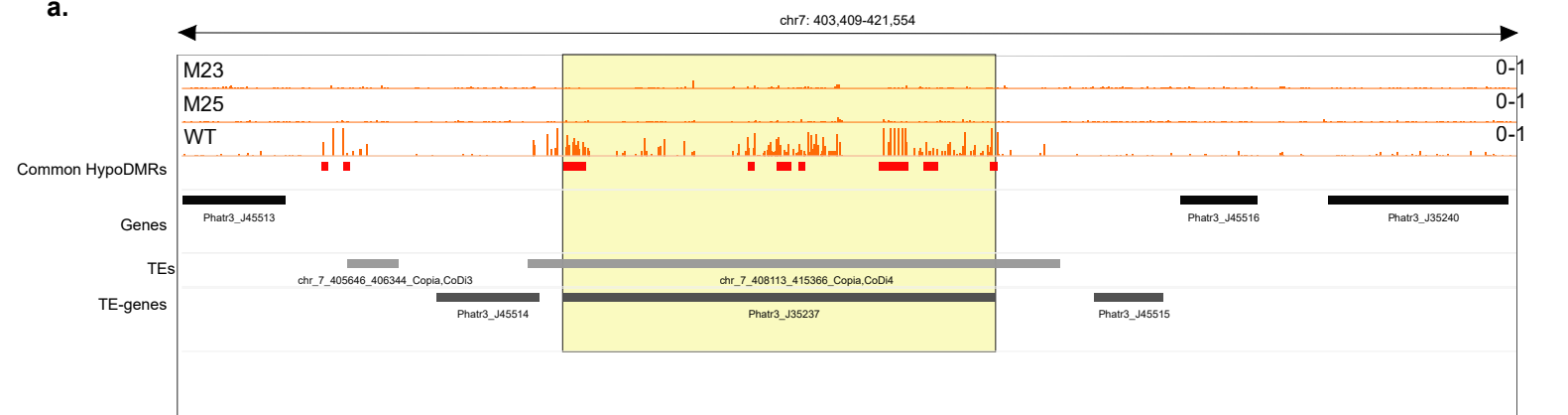


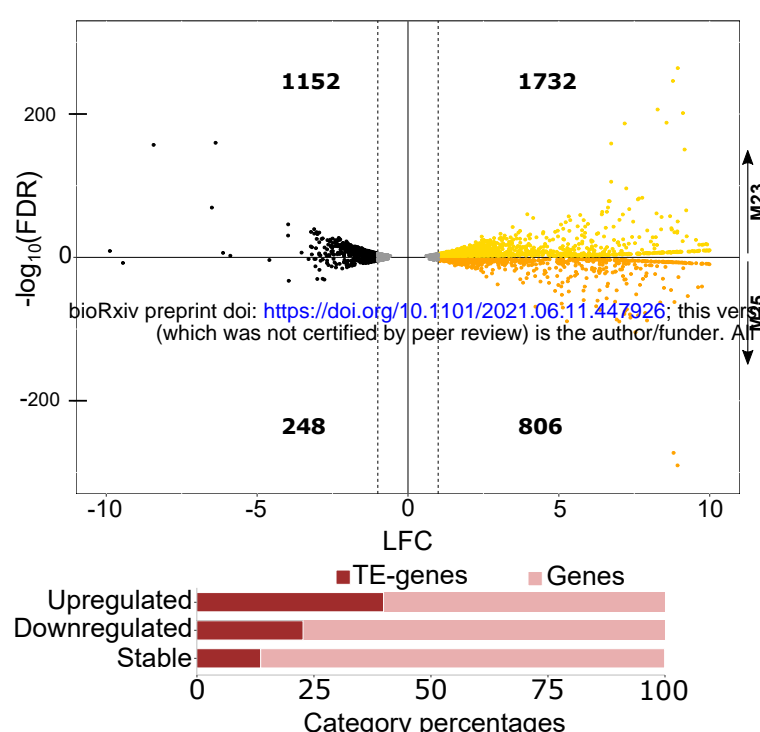
Fig. 3

CG methylation profiles in DNMT5-KO lines

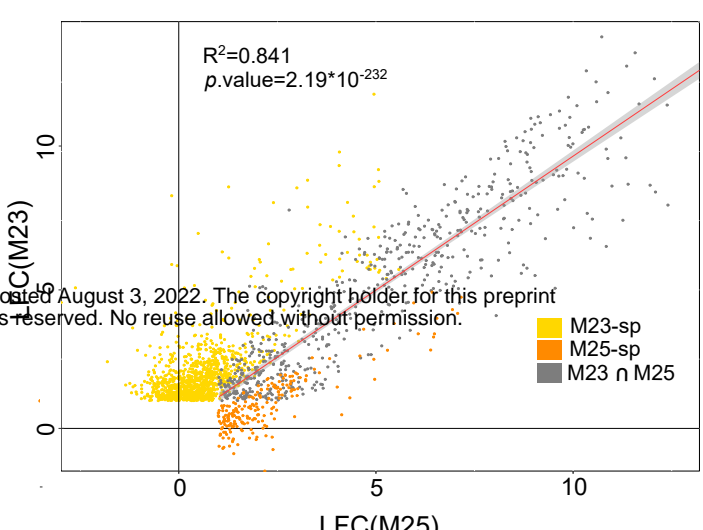
a. Heatmap of CG methylation levels in Pt18.6 reference (WT), M23 and M25 for TEs (left panel) and genes (right panel). **b.** Violin plot showing the methylation levels in all CGs found in TEs and genes in Pt1.86 and M25, M23. **c.** Venn diagram displaying the number of hypoDMRs identified in M23 (M23-spe) (yellow) and M25 (M25-spe) (orange). **d.** Percentages of overlap between common hypoDMRs, genes and TEs. **e.** Association between common hypoDMRs and regions targeted by histone post-translational modifications representative of the epigenetic landscape of *P. tricornutum*. The number of overlapping common hypoDMRs is shown for each histone modification and each combination of histone modifications.



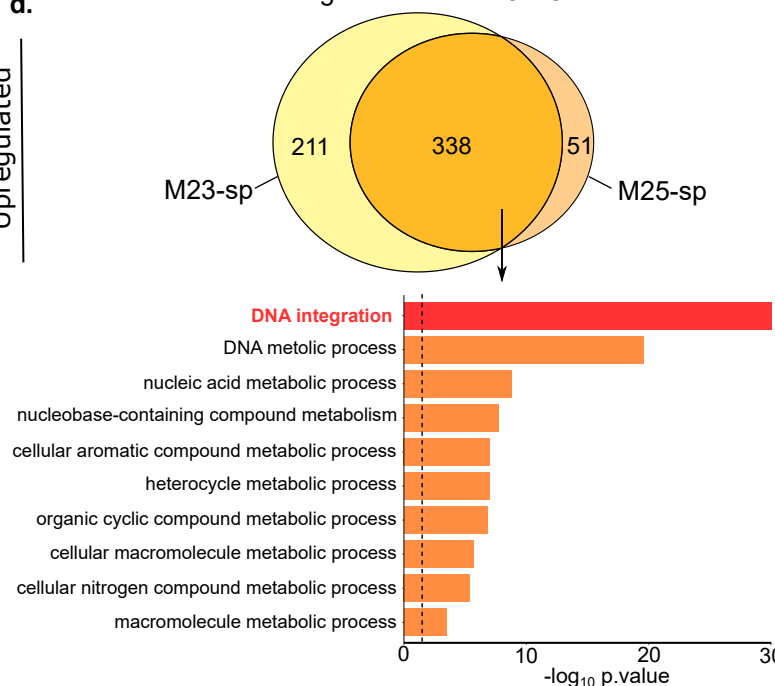
b.



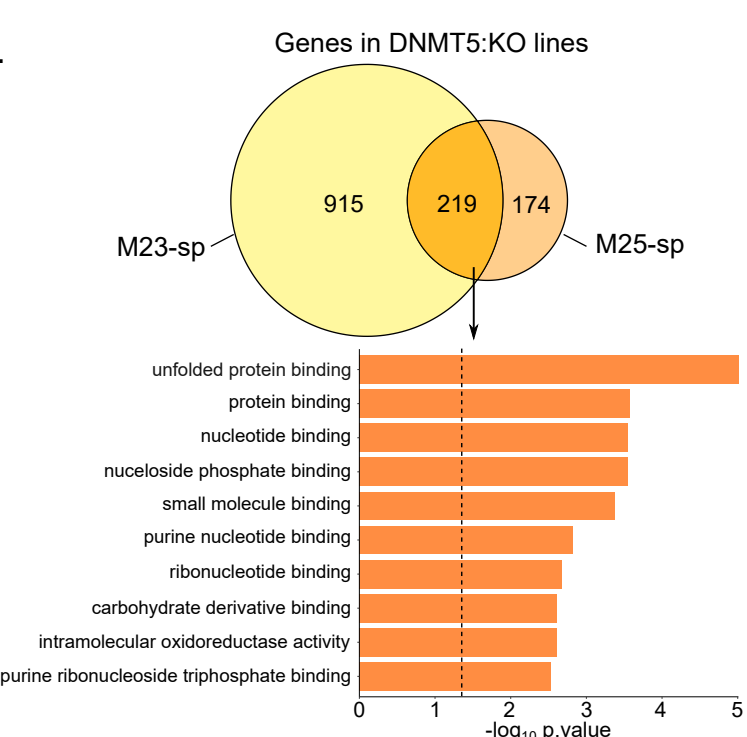
c.



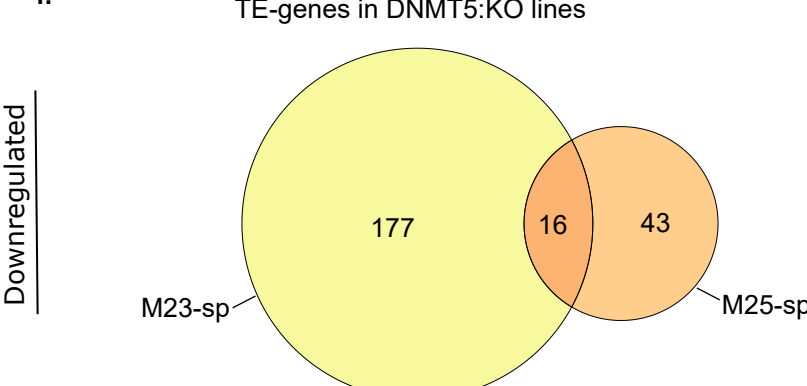
d.



e.



f.



g.

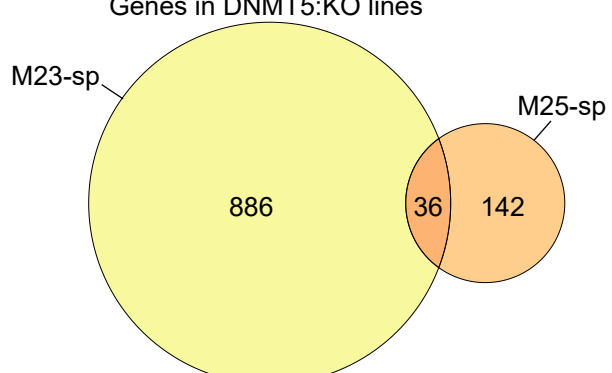


Fig. 4

Dynamics of gene and TE-gene expression in DNMT5:KO lines

a. Snapshot of an example TE-gene CG methylation profile. b. Differential expression in DNMT5:KOs (M23 and M25 are represented in the upper and lower parts of the volcano plot, respectively) compared with Pt18.6 reference (WT). The upper panel shows a volcano plot that displays the distribution of the fold changes (LFC) in the X-axis and adjusted p.values (-log₁₀FDR) in the Y-axis. The number of genes up and downregulated in each mutant are indicated. The stable genes (1 < LFC > -1 and FDR < 0.01) are shown in grey. The lower panel shows a bar plot that displays the proportion of genes and TE-genes in each expression category (downregulated, stable and upregulated). c. Scatter plot comparing fold changes of M23 and M25 upregulated genes. Yellow and orange dots represent specific significantly upregulated genes in M23, M25, respectively (LFC > 1 and FDR < 0.01, M23-sp, M25-sp, respectively). Grey dots represent significantly upregulated genes in both mutants (LFC > 1 and FDR < 0.01, M23 ∩ M25). The solid line represents the linear fit and the grey shading represents 95% confidence interval for the significantly upregulated genes in both mutants. d. and e. The upper panel represent Venn diagrams showing the numbers of specific (M23-sp, M25-sp) and common (M23 ∩ M25) upregulated TE-genes and genes, respectively, in each mutant compared to the Pt18.6 reference (WT). The lower panel shows the top 10 enriched canonical pathways of upregulated TE-genes and genes, respectively, sorted by p.value in both mutants (M23 ∩ M25) as identified by topGO analysis. The dashed lines show the p.value of 0.05. f. Venn diagram displaying downregulated TE-genes (LFC < -1 and FDR < 0.05) in M23 (M23-sp) (yellow) and M25 (M25-sp) (orange). g. as for f. for downregulated genes.

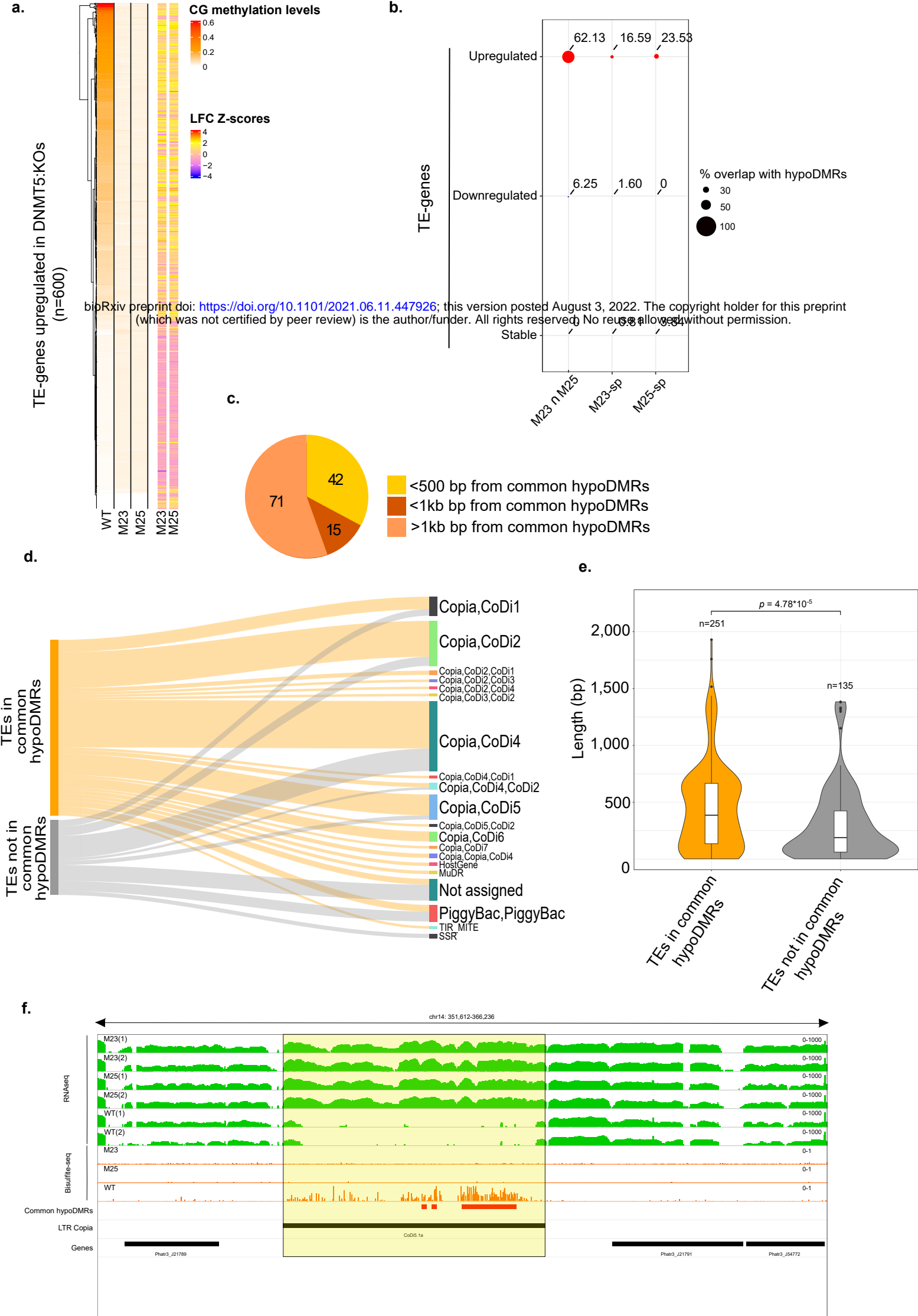
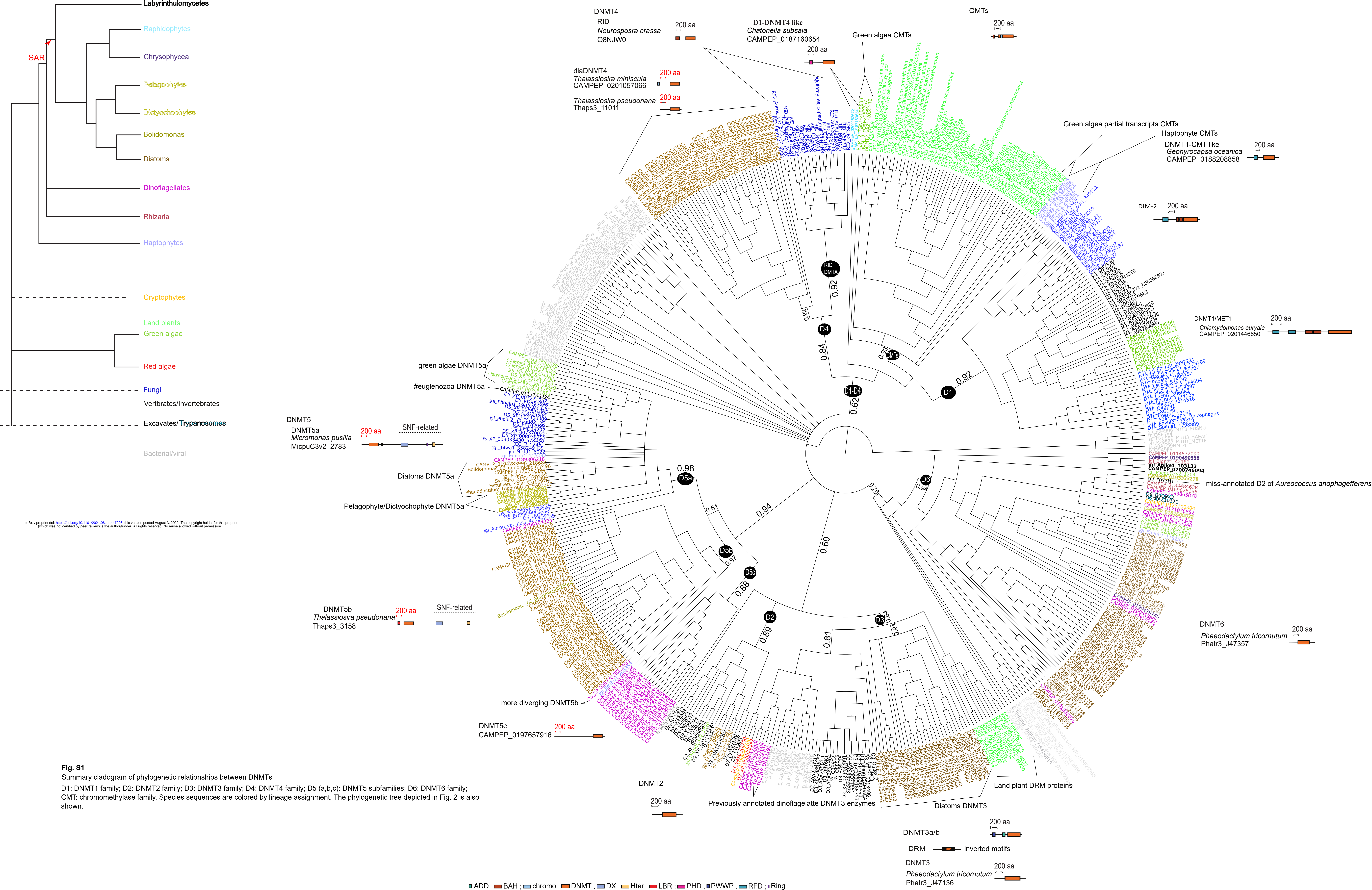


Fig. 5

Interplay between CG methylation and TE-gene expression

a. Heatmap of CG methylation levels in Pt18.6 reference (WT), M23 and M25 (left panel) and LFC normalised levels (Z-scores) (right panel) of the 600 upregulated TE-genes in M23 and M25 compared to Pt18.6 reference (WT). **b.** Percentages of overlap between common hypoDMRs and upregulated (red), downregulated (blue) and stable TE-genes (grey) in M23 only (M23-sp), M25 only (M25-sp) and both mutants (M23 ∩ M25). **c.** Distribution of common (M23 ∩ M25) upregulated TE-genes that overlap with TE-genes regulatory regions. **d.** Mapping of TEs covered in TE-genes that overlap or not with common hypoDMRs (queries in the left) onto annotated TEs on Phatr3. Bar sizes are proportional to the number of TEs in the queries that are assigned to each TE category. **e.** Violin plot comparing the length (bp) of TEs covered in TE-genes that overlap or not with common hypoDMRs. **f.** IGV snapshot of expression levels in both replicates of WT and DNMT5:KOs (M23 and M25) (green tracks) and CG methylation levels in the WT and DNMT5:KOs (M23 and M25) (orange tracks) of an example LTR copia (highlighted in yellow). The common hypoDMRs and genes are also shown in the red and black tracks, respectively.



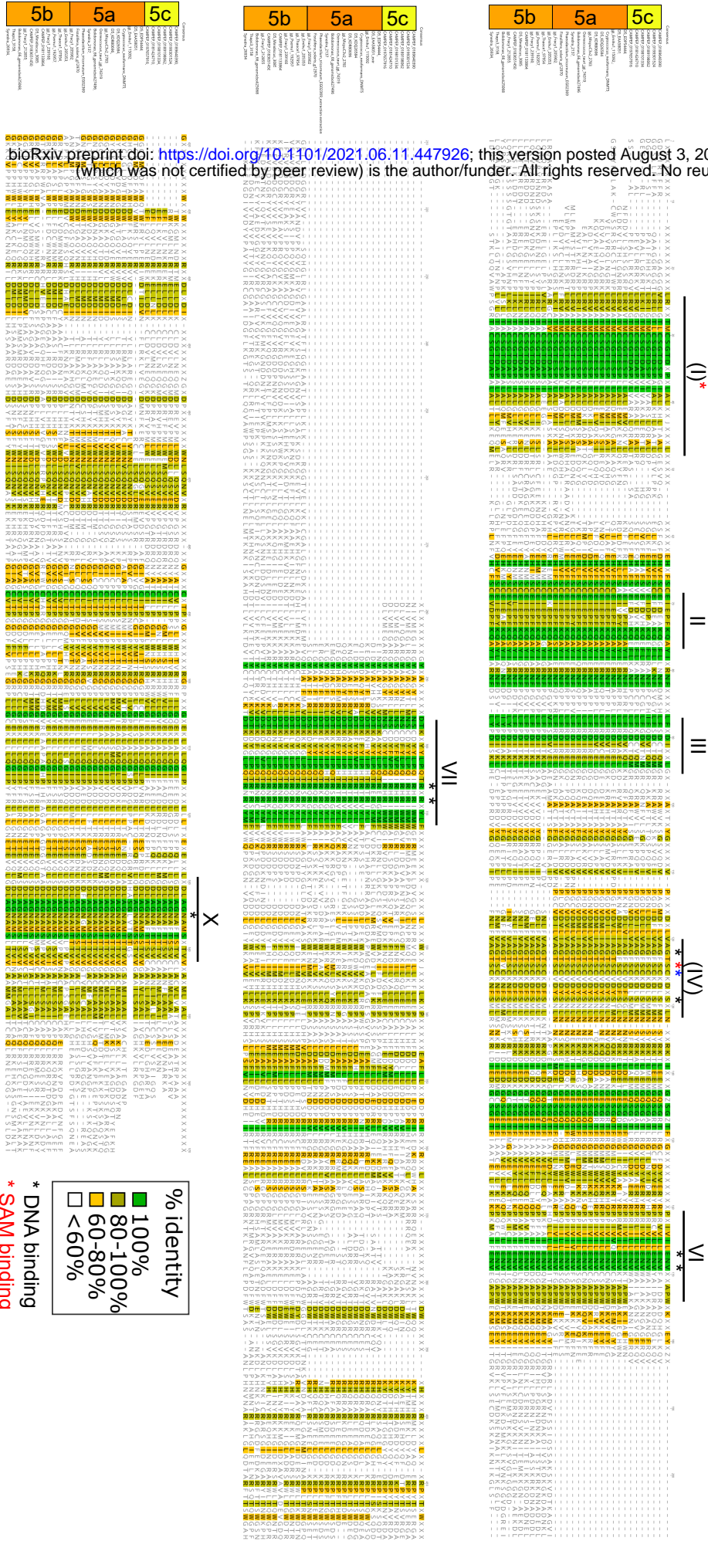


Fig. S2

Alignment of the DNM1 domain of representative DNM15 proteins

DNMT motifs are labelled using Roman numerals. Motifs put in brackets are divergent compared to other DNMTs. An annotation is proposed for the motif I: TxCSGTD(A/S)P and IV: TSC; that are highly divergent compared to other DNMT motifs I (DXFXGXG) and IV (PCQ); based on their conservation in other DNMT5s and their position relatively to the other conserved DNMT motifs. Other motifs are well conserved and amino acids with DNA binding function and SAM binding activity are annotated accordingly.

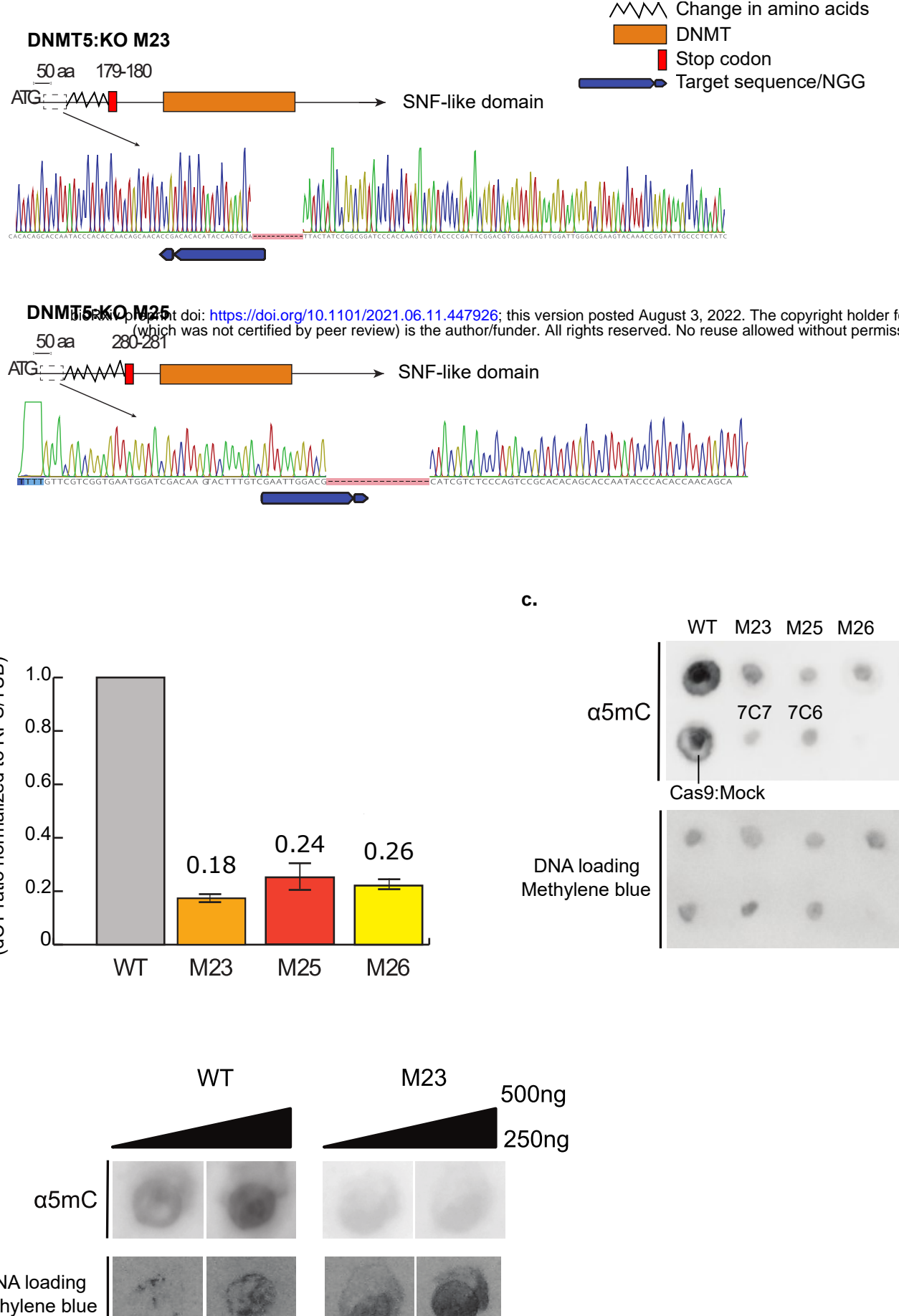
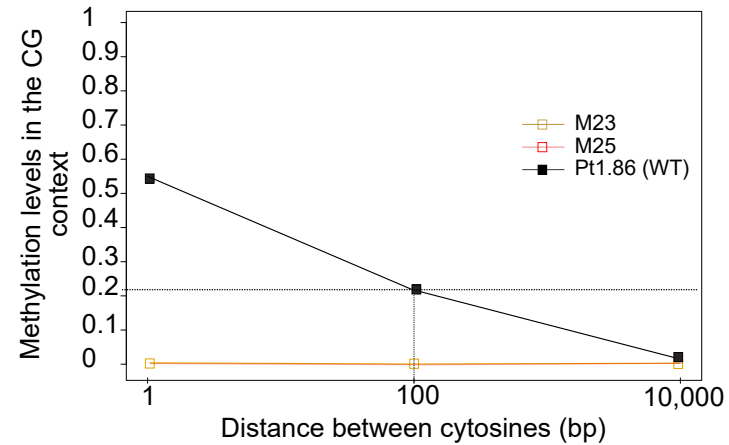
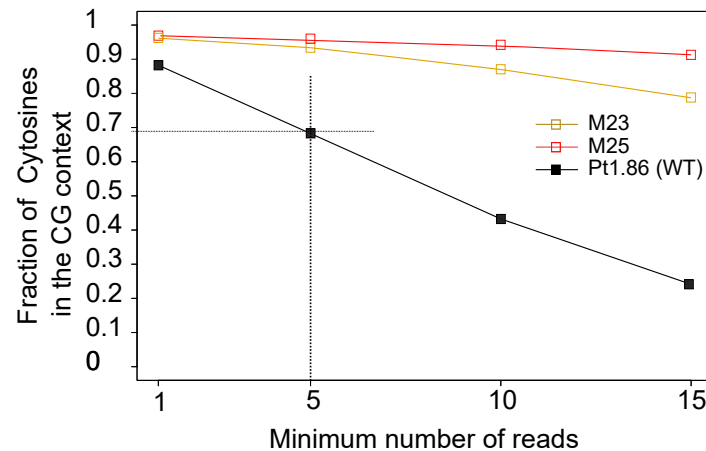


Fig. 63

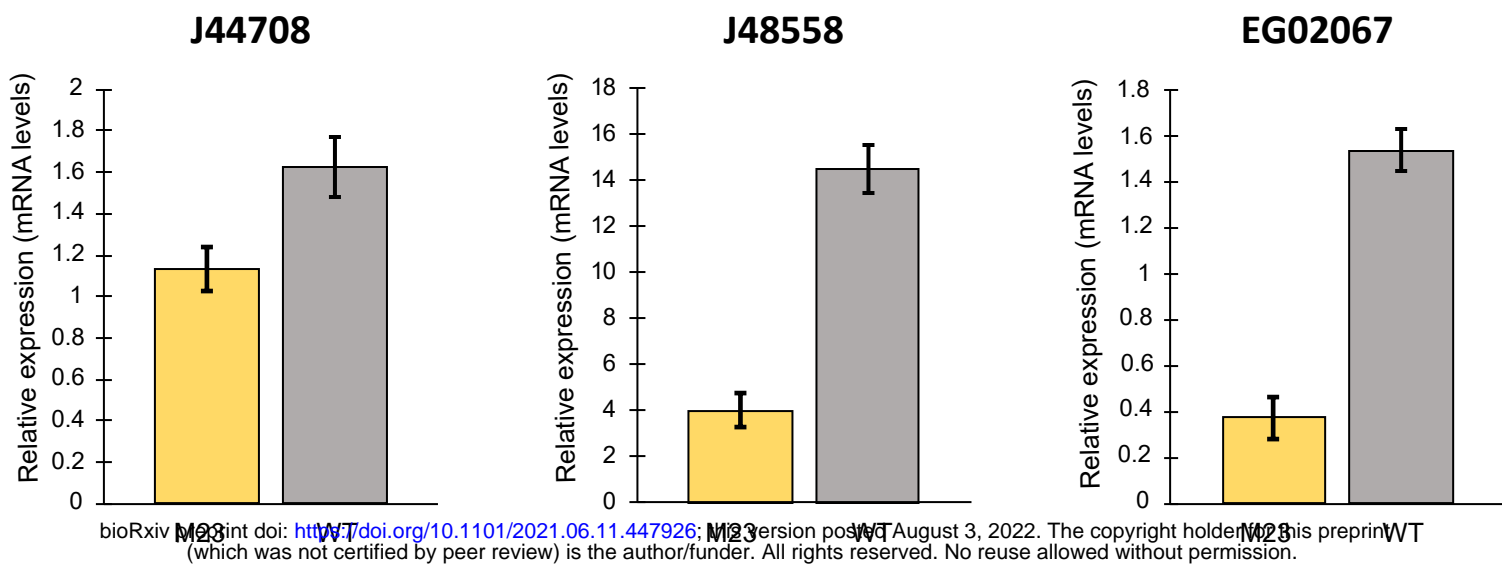
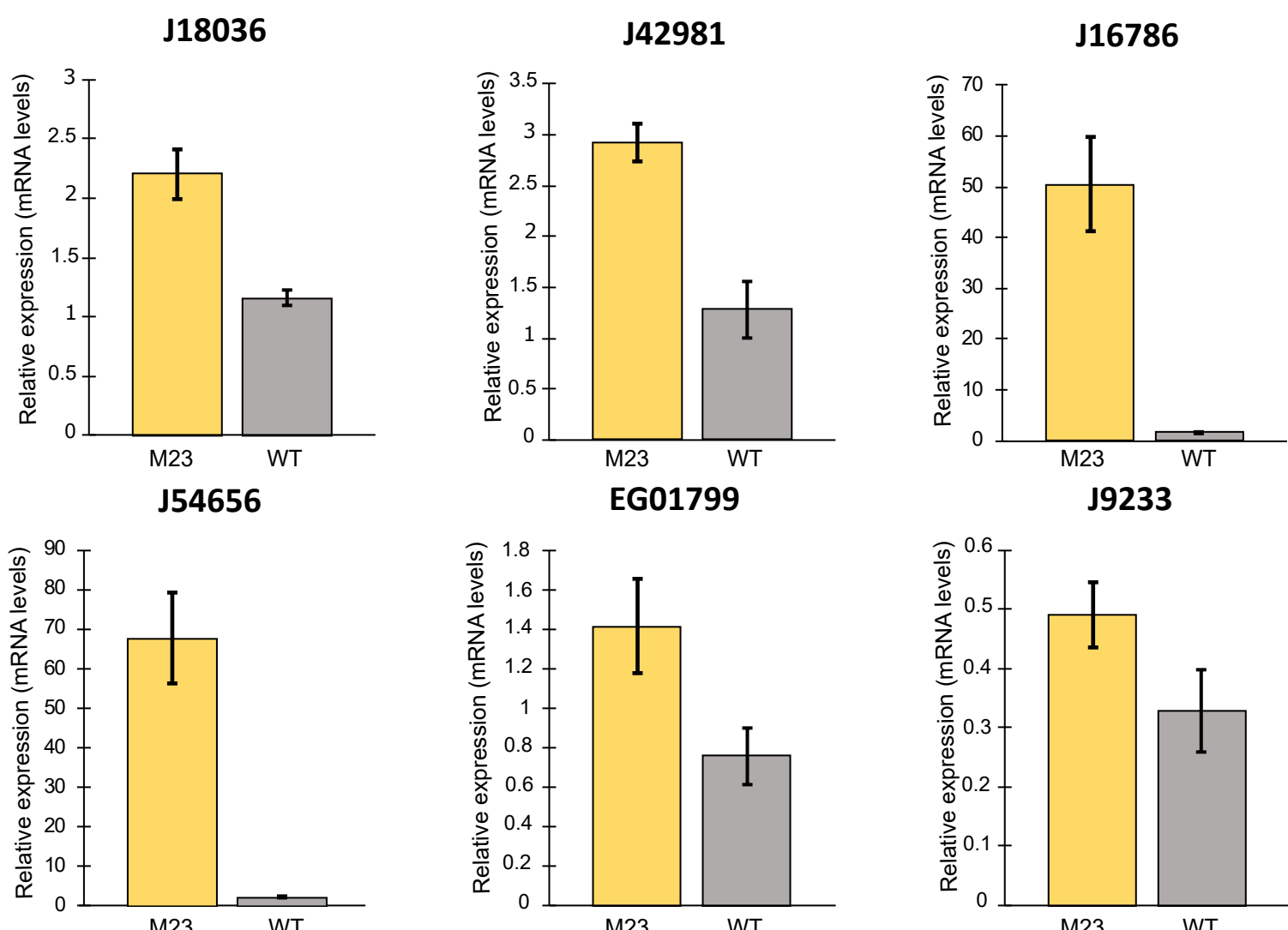
Fig. S3
DNMT5-KO cell lines

a. Homozygous mutations generated by CRISPR/Cas9 in M23 and M25 lines at two independent target sequences. In M25, the mutation consists in 16 base pair out of frame deletion around CRISPR/Cas9 cutting sites that generates a loss of amino acids from position 28 to 34 leading to a premature STOP codon at amino acid 280. The M23 cell line has a 11 base pair out of frame deletion that generates a loss of amino acids 58 to 60/61 followed by a premature STOP codon at amino acid position 179 -180 from ATG . **b.** Quantitative PCR analysis of DNMT5 mRNA levels in the mutants compared to the reference Pt18.6 line (WT). Average fold loss is calculated by the ratio of CTs, normalized on the RPS and TUB genes (see material and methods), between mutants and WT. Normalized ratios were then averaged on biological replicates (n=2) per line (*2 technical replicates per biological replicate) for 5 primers targeting all the DNMT5 transcripts. Error bars represent the standard deviation between biological replicates. DNMT5:KO M26 is an independent DNMT5:KO mutant showing a deletion at the same position of DNMT5:KO M23 and is not further described in this manuscript **c.** Dot blot analysis of DNMT5 mutants compared to the Pt18.6 reference line (WT) and the Cas9:Mock control. 7C4 and 7C6 are DNMT5:KOs mutants that were not further used in this study. No DNA methylation, compared to the reference strain, in any DNMT5:KO mutant could be detected. **d.** as for **c.** with serial dilutions of DNMT5:KO M23 genomic DNA. Background levels of DNA methylation are observed. Loading control is obtained by methylene blue staining.

a.**b.****Fig. S4**

Bisulfite sequencing features in the reference Pt18.6 and DNMT5:KO lines (M23, M25)

a. CG DNA methylation levels related to distance between cytosines in the reference Pt18.6 and DNMT5:KOs (M23, M25). DNA methylation levels sharply decline after 100 bp distance in the reference strain suggesting a sparse methylation pattern. No DNA methylation is found in DNMT5:KOs. **b.** Cytosine Coverage, after bisulfite treatment and Illumina sequencing in Pt18.6 and DNMT5:KOs, show a deeper cytosine coverage for mutants. The number of covered cytosines quickly drop in the reference strain above 5X, this threshold was chosen for subsequent analysis.

a.**b.****Fig. S5**

Quantitative PCR analysis of selected up and downregulated genes

a. Quantitative PCR analysis of mRNA levels of downregulated genes in the DNMT5:KO M23 compared to the reference Pt18.6 line (WT). Average fold loss is calculated by the ratio of CTs, normalized on the RPS and TUB genes (see material and methods), between mutants and WT on biological replicates (n=2) (*2 technical replicates per biological replicate). Error bars represent the standard deviation between biological replicates. **b.** as for **a.** for upregulated genes. Biological functions of tested genes can be found in Table S15.